AD-A127 402 TITANIUM MATRIX/CONTINUOUS FIBER COMPOSITE INTERFACE INTERACTIONS AND THE.. (U) TEXAS UNIV AT AUSTIN MATERIALS SCIENCE AND ENGINEERING H L MARCUS 25 FEB 83 1/1

UNCLASSIFIED UTMSE-83-2 AFOSR-TR-83-0243 AFOSR-80-0052 F/G 11/4 NL

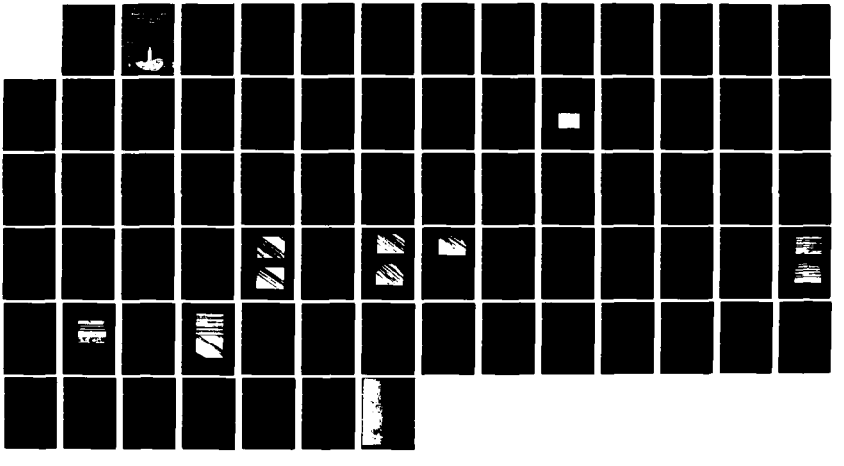

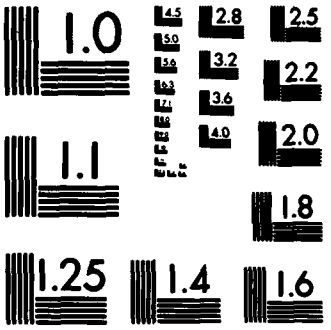

MICROCOPY RESOLUTION TEST CHART
NATIONAL BUREAU OF STANDARDS-1963-A

AD-A127 243

Science and Engineering

University of Texas at Austin

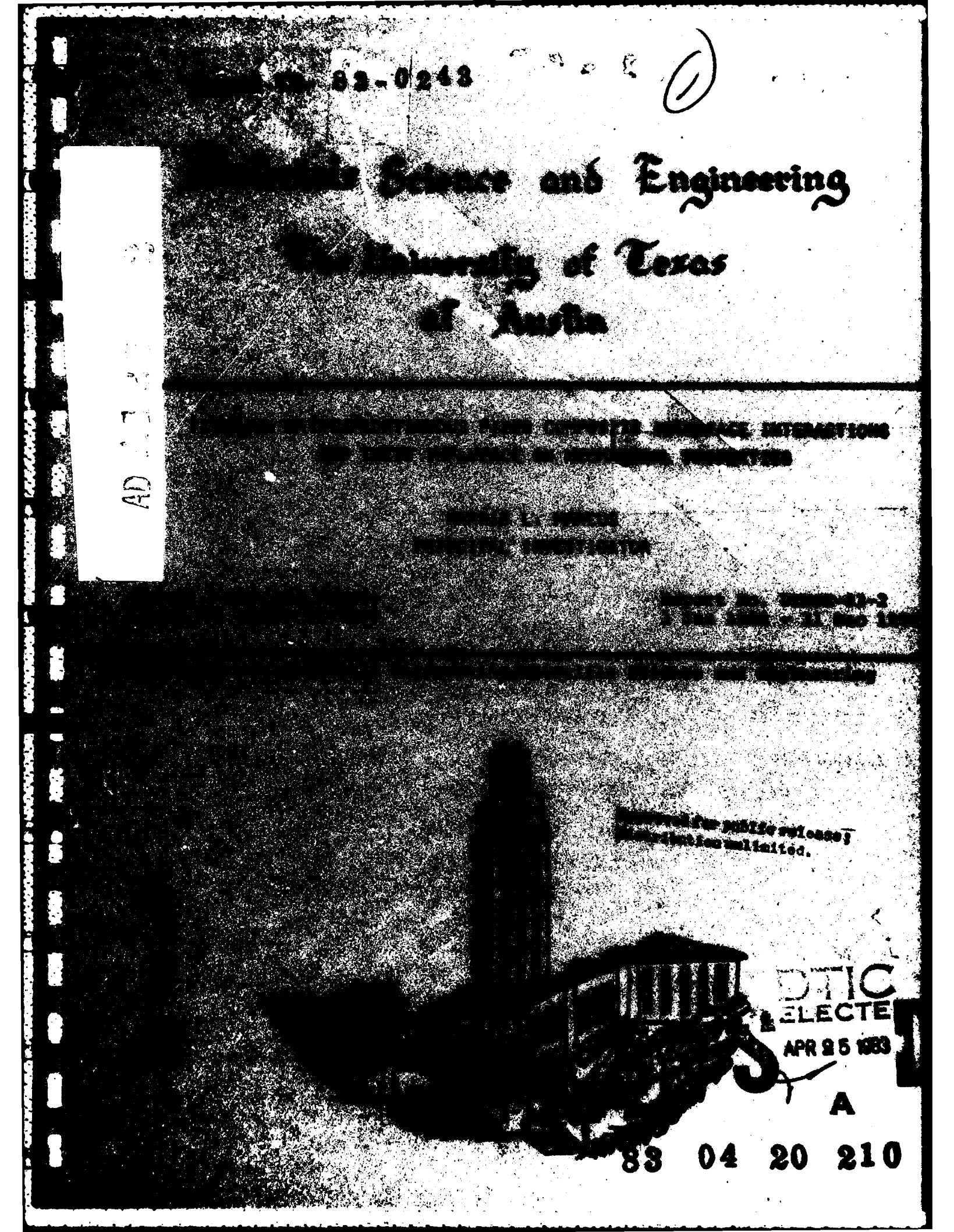

Annual Technical Report
Grant No. AFOSR 80-0052
The University of Texas at Austin
Interim Reporting Period: 1 January 1982 - 31 December 1982

TITANIUM MATRIX/CONTINUOUS FIBER COMPOSITE INTERFACE INTERACTIONS AND THEIR INFLUENCE ON MECHANICAL PROPERTIES

Principal Investigator

Harris L. Marcus, Professor
Mechanical Engineering/Materials Science and Engineering

Report Number: UTMSE-83-2

UNCLASSIFIED

SECURITY CLASSIFICATION OF THIS PAGE (When Data Entered)

REPORT DOCUMENTATION PAGE	READ INSTRUCTIONS BEFORE COMPLETING FORM
1. REPORT NUMBER: AFOSR-TR- 83-0243	2. GOVT ACCESSION NO. A127402	3. RECIPIENT'S CATALOG NUMBER
4. TITLE (and Subtitle): Titanium Matrix/Continuous Fiber Composite Interface Interactions and Their Influence on Mechanical Properties	5. TYPE OF REPORT & PERIOD COVERED: Annual Technical Report 1 Jan 1982 - 31 Dec 1982
	6. PERFORMING ORG. REPORT NUMBER: UTMSE- 83-2
7. AUTHOR(s): H.L. Marcus	8. CONTRACT OR GRANT NUMBER(s): AFOSR 80-0052
9. PERFORMING ORGANIZATION NAME AND ADDRESS: Department of Mechanical Eng/MS&E The University of Texas at Austin Austin, TX 78712	10. PROGRAM ELEMENT, PROJECT, TASK AREA & WORK UNIT NUMBERS: 61102F 2306/A1
11. CONTROLLING OFFICE NAME AND ADDRESS: Department of the Air Force AFOSR/NE, Air Force Office of Scientific Research Bolling, AFB, DC 20332	12. REPORT DATE: 25 February 1983
	13. NUMBER OF PAGES: 69
14. MONITORING AGENCY NAME & ADDRESS (if different from Controlling Office)	15. SECURITY CLASS. (of this report): Unclassified
	15a. DECLASSIFICATION/DOWNGRADING SCHEDULE

16. DISTRIBUTION STATEMENT (of this Report)

Approved for public release and distribution unlimited.

17. DISTRIBUTION STATEMENT (of the abstract entered in Block 20, if different from Report)

18. SUPPLEMENTARY NOTES

19. KEY WORDS (Continue on reverse side if necessary and identify by block number)

fracture, fatigue crack growth, titanium metal matrix composites, environmental effects, fatigue, AES, thermal fatigue, mixed mode fracture, SiC, B_4C/B, Interface diffusion

20. ABSTRACT (Continue on reverse side if necessary and identify by block number)

The effect on the fatigue crack growth behavior of the SiC and B_4C/B reinforced titanium-6 aluminum-4 vanadium metal matrix composites by the modification of the interface between the fiber and the matrix by isothermal and thermal fatigued treatments was studied. The thermal cycling and isothermal treatments were carried out in environments of vacuum, air and sulfur. One and two dimensional analysis of sulfur and oxygen diffusion indicated that the interface has a thin but finite thickness and is a high diffusion ...

DD FORM 1 JAN 73 1473 EDITION OF 1 NOV 65 IS OBSOLETE

UNCLASSIFIED

SECURITY CLASSIFICATION OF THIS PAGE

20. Abstract continued.

path for sulfur and oxygen. Thermal cycling treatment enhanced the interface diffusion.

The fatigue crack growth results demonstrated that the interface transferred the load during fatigue cycling in either an inert environment or if the interface has a minimal amount of impurities. In the case of the sulfur enriched interface the humid air, FCG environment reduced the cohesion of the interface with the load totally carried by the matrix. This led to an increased FCG rate with a higher value of the Paris exponent. Without the enhanced sulfur at the interface the Paris exponent remained constant although the fatigue crack growth rate nominally increased in humid air environment. The fatigue crack growth rate in dry hydrogen was lower than in the humid air but greater than in dry nitrogen for all conditions. In some of the cases the total FCG rate change could be explained in terms of the volume fraction of the matrix relative to FCG of the monolithic Ti-6Al-4V matrix material.

A thermodynamic model on the impurity effect on interface cohesion is presented that will be tested relative to the modifications in interface chemistry.

INDEX

TITANIUM MATRIX/CONTINUOUS FIBER COMPOSITE INTERFACE INTERACTIONS AND THEIR INFLUENCE ON MECHANICAL PROPERTIES

I. Introduction

Filamentary metal-matrix composites have generated a considerable amount of interest in the materials field because of their potential applications in dynamic structures. A metal matrix composite system (MMC) carries certain distinct advantages over other composite systems. High strength, modulus, toughness, surface durability, and low notch sensitivity are just a few of these potential advantages over other composite systems.

Titanium metal matrix composites are attractive for applications requiring a stronger matrix and higher temperature capability than other metal matrix composites. Applications requiring high stiffness and low weight in the 450-900°K temperature range will benefit from the development of titanium matrix composites.

In the research reported on here, various experiments are being done to study the effects of temperature and other environments on the interfaces and the mechanical properties of the titanium metal matrix composites reinforced with SiC, Borsic or B_4C-B fibers. Specimens of longitudinal and transverse fiber orientation as well as angled to the loading axis were used.

The mechanical properties studied are mixed mode loading residual strength after thermal and thermal fatigue exposure and fatigue crack growth under Mode I and Mixed Mode loading after thermal treatment. The condition of the matrix fiber interface as a function of the above

treatments is characterized with both Scanning Auger Microscopy (SAM) and Scanning Electron Microscopy (SEM). The fiber interface chemistries were modified by thermal treatment in oxygen and sulfur bearing environments.

The composite materials used in this investigation are Ti-6Al-4V metal matrix reinforced with about 40 V%, Borsic, B_4C/B or SiC filaments. Materials were obtained in the form of sheet panels through the Air Force Materials Laboratory. The composite panel was cut by electric-discharge-machine (EDM) into specimens.

II. Results and Discussion

The major results obtained during this reporting period are given in great detail in Appendices A-D. In this part of the report the key observations will be summarized and the reader will need to see the appendices for the details. Appendix A focuses on the analysis of the diffusion of oxygen and sulfur during thermal exposure. Appendix B describes an analysis of the Auger electron spectroscopy data to give more accurate surface chemical analysis. Appendix C details the experimental results of fatigue crack growth measurements in Ti/SiC and Ti/B_4C/B metal matrix composites. Appendix D is a thermodynamic approach to interface cohesion as influenced by segregation.

A. Interface Diffusion Studies

Interface diffusion was studied under two conditions. The first was for isothermal heat treatment and the second was for equivalent time at the elevated temperature but thermal fatigue cycled. The environmental exposure was to 50% R.H. air and to sulfur vapor. The

diffusion down the interface was enhanced under the thermal cycling conditions. The 550°C sulfur interface diffusion coefficient was found to be $5x10^{-9}$ cm^2/sec for the SiC composites and $7x10^{-9}$ cm^2/sec for the interface diffusion of oxygen down the B_4C/B composite interface. The fracture at the interface showed branch cracking in the matrix side of the interface the full extent of the sulfur diffusion path. Another observation of interest was the high surface mobility of the sulfur. It was shown to diffuse over the matrix fracture surface between the fibers, a point of importance in the fatigue crack growth studies to be discussed later.

In addition to the diffusion down the interface, diffusion into the matrix was studied with combined AES and inert ion sputtering. The two-dimensional diffusion problem was evaluated using a model by Fisher and is described in detail in Appendix A. The diffusion into the bulk was analyzed for the case of thermal cycling. In carrying out this analysis the influence of the layer thickness on the quantitative analysis of the AES data was evaluated using an analysis by Stevens as described in detail in Appendix B. The use of AES to determine the diffusion profiles also allowed determination of the fracture path. The following summarizes the results for the fracture path and diffusion analysis.

1) Samples thermal cycled in air between RT and 550°C for one day have high concentration peaks of oxygen at the interface near the exposed surfaces and diffused some distance into the interface. The isothermal treatment in air does not significantly increase the oxygen level on the interface. The reduction of longitudinal fracture

strength and the fracture mode changes in the titanium MMCs are attributed to the higher amount of oxygen and sulfur in the interface for the specimen thermal cycled in air and sulfur environment.

2) Thermal cycled SiC/Ti-6Al-4V specimens showed a greater amount of oxygen and sulfur in the matrix side of the interface and virtually none on the fiber side. This shows the fracture path to be between the sulfide or oxide and the fiber in the interface.

3) B_4C/B/Ti-6Al-4V specimens have a strong TiB_2 peak on the matrix side of the fractured interface. This indicates that the fracture occurred at the B_4C and TiB_2 interface.

4) The plot of logarithm of sulfur concentration vs. distance measured from the end of the specimen allowed a straight line fit to the data for thermal cycled specimens as follows:

$$\ln S_s = kz$$

A similar trend was also noted from the oxygen profile. Results from an isothermal treatment did not give a straight line relationship.

5) The two-dimensional diffusion problem was evaluated based on the grain boundary diffusion equation. The rapid diffusion down the boundary was separated from the slow diffusion into the bulk resulting in two one-dimensional analyses.

6) The sulfur diffusion down the interface was far larger than that into the bulk, a 10^5 difference in diffusion distance, confirming that the interface provides a high rate diffusion path for environmental elements. The diffusion coefficient of sulfur down the interface was calculated to be 5×10^{-9} cm^2/sec at a maximum temperature of 550°C during thermal cycling for SiC/Ti-6Al-4V composites.

7) The oxygen diffusion coefficient was calculated to be 7×10^{-9} cm^2/sec for B_4C/B/Ti-6Al-4V composites thermal cycled in air for one day between RT and 550°C.

8) The sulfur detection distance was about 500 μm after one day thermal cycling treatments. The branch cracks from SEM fractography extend an equivalent distance to it. The interface cracking normal to the propagating main crack is associated with the thin but finite sulfide layer at the interface.

9) From the Arrhenium relationship used to determine the activation energy for the diffusion process, the activation energy of oxygen diffusion was 8 Kcal/mole and that of sulfur was 15 Kcal/mole, which are far below the activation energy for the bulk diffusion and are consistent with the interface diffusion mechanism.

10) The enhanced degradation of the interface by sulfur and oxygen during thermal cycling when compared to isothermal heat treatment may be explained by dislocation transport along the interface of the sulfur or oxygen. The dislocations are present due to the thermally induced plastic deformation near the interface during the thermal cycling.

B. Fatigue Crack Growth of SiC and B_4C/B-Ti MMC

The fatigue crack growth behavior in Ti-MMC was described in the last report in terms of the environment and mixed mode loading conditions. During the present reporting period, the fatigue crack growth (FCG) behavior of SiC and B_4C/B reinforced titanium metal matrix composites loaded in the transverse direction was studied as a function of interface modifications and gaseous environments. This was investigated to determine if the change in interface chemistry and strength, which were modified by the diffusion of sulfur during thermal cycling, resulted in a change in the FCG behavior. Also studied was the effect of various gaseous environments such as humid lab air, dry nitrogen and dry hydrogen on the FCG rate. The heat treatment employed consisted of thermal cycling the composite specimens between RT and 550°C for 84 hours in an environment of sulfur. The details are given in Appendix C and are outlined in the following.

Experiments were carried out on both as-received and thermal cycled SiC/Ti-6Al-4V specimens in laboratory air of 50% R.H. The rate of crack growth in the heat treated specimens exceeded that of the as-received specimens indicating that the thermal cycling in S degraded the fatigue resistance. Fractography on the as-received specimen indicated the presence of both fiber splitting and interfacial debonding while the heat treated specimens showed only interfacial debonding.

Additional FCG experiments were performed in dry N_2. Both the as-received and thermal cycled specimens showed considerably lower FCP rates in N_2 than in humid air although there was no conclusive difference in the FCP rates of the two sets of specimens in N_2. Fiber splitting was seen for both conditions in contrast to previous results for BORSIC/Ti-6Al-4V where fiber splitting occurred only in humid air. This difference was attributed to either the better fiber matrix bonding in the SiC composites or to the increased brittleness of SiC fibers causing them to split in preference to debonding from the matrix.

FCG tests for as-received B_4C/B/Ti-6Al-4V transverse specimens cyclically loaded at a load ratio, R=0.1 in 50% RH air showed higher growth rate in humid air. Fatigue crack growth results conducted on the Ti-6Al-4V alloy in humid air and inert dry argon at room temperature yielded almost identical cyclic crack growth rates (Ref. 2, Appendix C). FCG rates tend to be higher in humid environments with an increased amount of fiber splitting. The FCG in dry N_2 environment, on the other hand, was more often by interface debonding with some fiber splitting and fiber fracture. Specimens thermal cycled in sulfur show higher FCG rates in lab air than the as-received sulfur free specimens with well-defined interface debonding. The Paris slope (m) is greater for those specimens.

The FCG results for the samples thermal cycled in a sulfur environment and tested in dry N_2 gas indicated a slight decrease in growth rate with the same Paris slope for the as-received specimens. With the exception of the samples thermal cycled in sulfur

and tested in humid air, the fracture strength is dominated by the crack growth resistance of the titanium matrix. In fact if it is assumed that all the cyclic stress and COD are accommodated by the matrix material the equivalent $\Delta K/E$ would translate the results to match the Ti-6Al-4V results.

The sulfur enriched interface of the specimen thermal cycled in sulfur reacts with the humidity in the air during FCG in lab air to degrade the interface cohesion resulting in complete separation of the interface from the matrix and the fiber at low strains. This total inability of the interface to sustain any strain further increases the fatigue crack growth rate in the matrix. The increase in the value of the slope may be due to the degradation of the interface by titanium sulfides creating a volume of brittle materials. This then leads to interface debonding and cracking as discussed earlier.

On the basis of the results of the experiments described above, a model for the failure mechanism for the FCG of the transverse titanium MMCs can be proposed. Due to the large anisotropy for the MMCs, the plastic zones in the matrix are elongated in the direction of the fibers. Thus the fibers in front of a sharp crack can be assumed to be surrounded by a plastic sheath of the matrix leading to interface or fiber fracture. In the case of the sulfur enriched specimen, fatigue cycling in humid air reduced the cohesion of the interface so the load is totally carried by the matrix. Necking occurs between the two adjacent fibers initiating from the rough interface surface due to the interaction of the titanium sulfide and the

humidity. The high surface mobility of sulfur discussed earlier is required for the enhanced FCG since the sulfur did not diffuse down the total interface.

Appendix D describes a thermodynamic model to explain the influence of impurities on the interface cohesion. In the case of the composites the fiber is considered to have very low solubility for the segregating element leading to the half plane analysis.

III. Summary

The effect on the fatigue crack growth behavior of the SiC and B_4C/B reinforced titanium-6 aluminum-4 vanadium metal matrix composites by the modification of the interface between the fiber and the matrix by isothermal and thermal fatigued treatments was studied. The thermal cycling and isothermal treatments were carried out in environments of vacuum, air and sulfur. One and two dimensional analysis of sulfur and oxygen diffusion indicated that the interface has a thin but finite thickness and is a high diffusion path for sulfur and oxygen. Thermal cycling treatment enhanced the interface diffusion.

The fatigue crack growth results demonstrated that the interface transferred the load during fatigue cycling in either an inert environment or if the interface has a minimal amount of impurities. In the case of the sulfur enriched interface the humid air, FCG environment reduced the cohesion of the interface with the load totally carried by the matrix. This led to an increased FCG rate with a higher value of the Paris exponent. Without the enhanced

sulfur at the interface the Paris exponent remained constant although the fatigue crack growth rate nominally increased in humid air environment. The fatigue crack growth rate in dry hydrogen was lower than in the humid air but greater than in dry nitrogen for all conditions. In some of the cases the total FCG rate change could be explained in terms of the volume fraction of the matrix relative to FCG of the monolithic Ti-6Al-4V matrix material.

A thermodynamic model on the impurity effect on interface cohesion is presented that will be tested relative to the modifications in interface chemistry.

IV. Future Research

The continuing effort will focus on the influence of gas environments on the FCG behavior of the composites whose interface is modified by sulfur. It was observed earlier that water vapor may be responsible for fiber embrittlement during FCG test. The embrittlement effect of the D_2 or D_2O gases can be evaluated with SIMS measurements. Further SAM work is planned in an attempt to characterize the matrix-fiber interface with reference to sulfur diffusion during thermal cycling to enable the AES correction to be made over the entire length of the diffusion path.

Quantitative mechanical peel test will be attempted for model layered SiC/interface/pure titanium composites. The interface chemistry will be chemically modified to simulate the continuous fiber composites. The mechanical behavior in different environments will then be evaluated.

V. Personnel Involved in Research 1982

Principal Investigator:

Harris L. Marcus
Harry L. Kent Jr. Professor of Mechanical Engineering

Others:

Professor John P. Stark
[served as an unpaid consultant on the thermodynamic modeling]

Michael Schmerling
Research Associate

Graduate Students

Young Hoon Park - Thermal Fatigue, Mixed Mode Fracture, Interface Diffusion

Doo Young Lee - Interface Segregation

Dushyant Narayen - Environmental Fatigue Crack Growth

VI. Dissertation

Deepak S. Mahulikar, "Effect of Environments on the Fatigue Crack Propagation Behavior of Titanium Metal Matrix Composites," December 1981, The University of Texas, Austin.

VII. Publications

1. D.S. Mahulikar, Y.H. Park and H.L. Marcus, "Mixed Mode Crack Propagation in Continuous Fiber Metal Matrix Composites," Proceedings of the Greece/USA Mixed Mode Fracture Conference, Athens, Greece; Sih, G.C. and Theocaris, P.S., Editors, Sijthoff and Noordhoff, p. 385 (1981).

2. D.S. Mahulikar, Y.H. Park and H.L. Marcus, "Environmental Influences on the Fracture and Fatigue Properties of Titanium Metal Matrix Continuous Fiber Composites," to be published in the ASTM-STP Proceedings of the 14th National Symposium on Fracture Mechanics, June/July 1981, Los Angeles.

3. Y.H. Park and H.L. Marcus, "Influence of Interface Degradation and Environment on the Thermal and Fracture Fatigue Properties of Titanium Matrix/Continuous SiC Fiber Composites," to be published in the Proceedings of the 6th Failure Modes in Composites, 1982, Dallas.

4. D.S. Mahulikar and H.L. Marcus, "Environmentally Influenced Mixed Mode Fatigue Crack Propagation of Titanium Metal Matrix Composites," to be published in Met. Trans.

5. D. Finello, Y.H. Park, M. Schmerling and H.L. Marcus, "Fractography of Metal Matrix Composites," to be published in ASTM-STP on Fractography in Failure Analysis of Ceramics and Metals, Philadelphia, PA, April 1982.

6. M. Schmerling and H.L. Marcus, "The Influence of Surface Roughness on the Electron Spectroscopy of Fractured Materials," to be published in SEM-82.

Talks

1. H.L. Marcus, Invited Talk, "Mixed Mode Crack Propagation in Continuous Fiber Metal Matrix Composites," Greece/USA Mixed Mode Fracture Conference, Athens, Greece, August 1980.

2. Y.H. Park, D.S. Mahulikar and H.L. Marcus, "Interfacial Degradation Due to Isothermal and Cyclic Thermal Treatment in Ti-6Al-4V Matrix Composites," 1981 Annual AIME Meeting, Chicago, February 1981.

3. D.S. Mahulikar, Y.H. Park and H.L. Marcus, "Environmental Influences on the Fracture and Fatigue Properties of Titanium Metal Matrix Continuous Fiber Composites," 14th National Symposium on Fracture Mechanics, ASTM-STP, June/July 1981, Los Angeles.

4. Y.H. Park and H.L. Marcus, "Influence of Interface Degradation and Environment on the Thermal and Fracture Fatigue Properties of Titanium Matrix/Continuous SiC Fiber Composites," 6th Failure Modes in Composites Conference, Dallas, February 1982.

5. H.L. Marcus, "The Influence of Impurity Elements on the Properties of Alloys," Joint TMS-AIME and BSD-ACS, Louisville, October 1981.

6. H.L. Marcus, Invited Talk, "Metal Matrix Composites," General Dynamics, Fort Worth, TX, January 19, 1983.

7. H.L. Marcus, Invited Talk, "Studies in Metal Matrix Composites," Aerospace Corporation, Los Angeles, December 1982.

8. Y.H. Park and H.L. Marcus, "An Interface Diffusion Study in Titanium Metal Matrix/Continuous B_4C/B Fiber Composites," to be presented AIME Annual Meeting, Atlanta, GA, March 1983.

Coupled Interactions

The following interactions involving our research took place in 1981 and 1982:

1. Continued discussions with Smith and Froes, AFML on program. AFML supplied material for studies.

2. Continued discussions and coordinated studies with Southwest Research Institute, Gerry Leverand, David Davidson and John Hack.

3. Discussions with Howard Katzman, Gary Steckle and George Kendall, Aerospace Corporation.

4. Discussions with Bill Harrington, DWA, Jim Cornie, AVCO LeRoy Davis, Netco.

5. Discussions with Bill Yee and group, General Dynamics.

6. Will attend ASTM meeting, Atlanta, March 1983.

Appendix A

Diffusion Analysis of Sulfur and Oxygen

A.1 One-dimensional diffusion analysis

The sulfur peak-to-peak height on the matrix side of the interface vs. distance from the end of the specimen for SiC/Ti-6Al-4V composites is plotted in Fig. 1. The peak-to-peak (p/p) height, $S_s(z)_{at\ y=0}$, should be converted to true concentration, $C_s(z)_{at\ y=0}$, as discussed in Appendix B. Since the sputtering was carried out only at one location into the bulk, that is, at $z=z_1$, the concentrations along the interface were obtained from the calculations using elementary sensitivity factors.[1] All profiles show ever decreasing amounts of sulfur toward the inside of the specimen. The profile of the specimen thermal cycled for one day shows a high concentration of sulfur near the end of the specimen. The plot of the logarithm of sulfur concentration vs. distance displayed a linear dependence of the data for the thermal cycled specimens as shown in Fig. 2. Therefore, the experimental results can be expressed as

$$\ln S_s = kz \qquad (1)$$

where S_s is the concentration of sulfur in the interface, z diffusion distance and k the proportionality constant. When the concentration of oxygen from samples thermal cycled in air is plotted as logarithm S_o against the distance from the end, the results show a similar trend. Fig. 3 shows the combined results from sulfur and oxygen

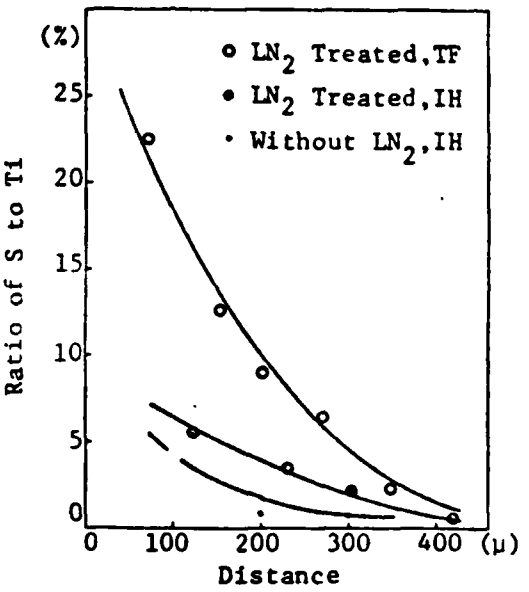

Figure 1. AES analysis of sulfur along the matrix side of interface for SiC/Ti-6Al-4V composites, thermal cycled (TF) and isothermally treated (IH).

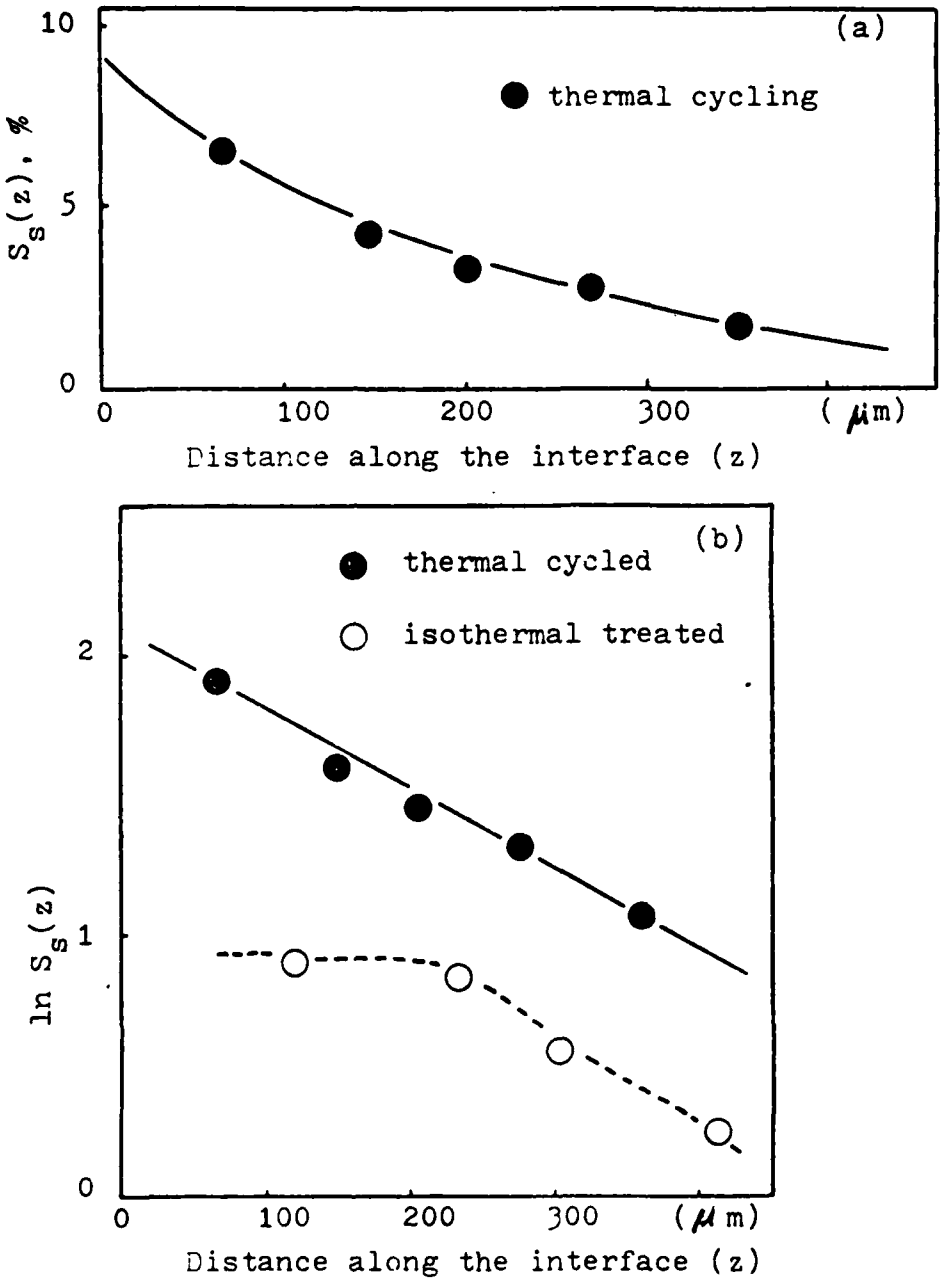

Figure 2. Sulfur concentration changes along the matrix side interface; (a) $S_s(z)$, (b) logarithm fitting of $S_s(z)$ for SiC/Ti-6Al-4V.

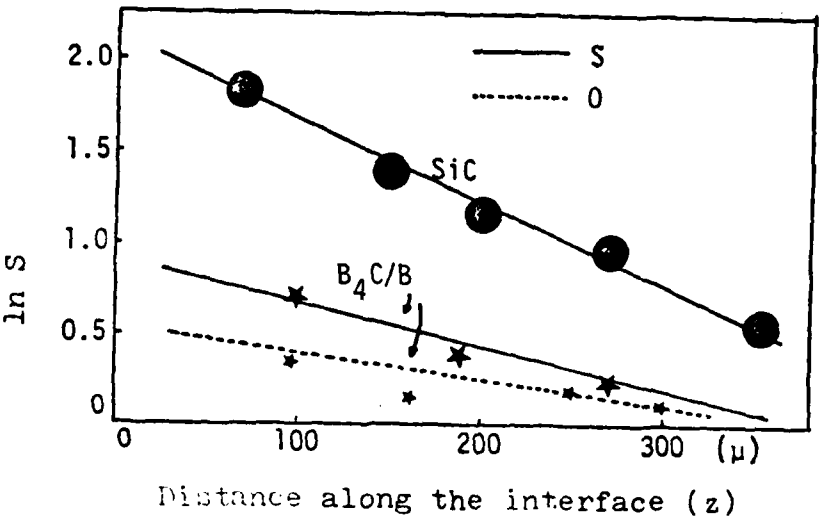

Figure 3. Logarithmic fitting of environmental element concentration along the matrix side interface, sulfur and oxygen, thermally cycled for 1 day between RT and 550°C.

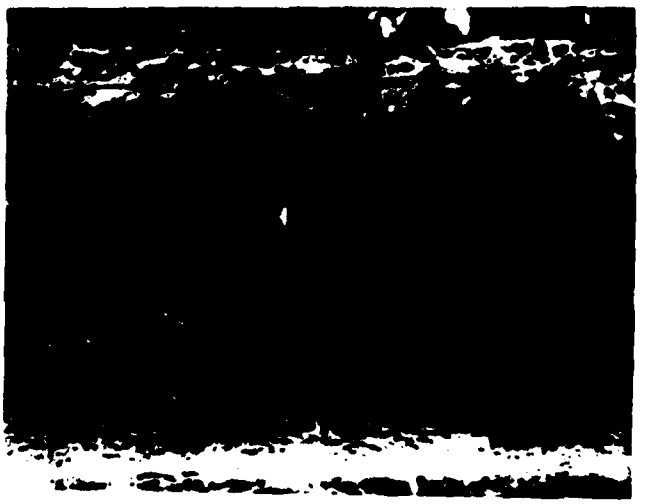

Figure 4. SEM fractograph of SiC/Ti-6Al-4V composite thermal cycled in sulfur for 1 day up to 550°C, showing branch cracks along the matrix side interface.

experiments. The slope is steeper for the sulfur environment, indicating enhanced sulfur reaction which is expected due to the higher vapor pressure and corresponding activity in the sealed pyrex tube, about 3.9 atm, at the maximum cycling temperature of 550°C. It is also noted that the diffusion rate of sulfur associated with thermal cycling is higher for the SiC fiber composite when compared with the B_4C/B fiber composite results. The oxide or sulfide formation at the interface during thermal cycling is due to the diffusion of oxygen or sulfur down the interface from the exposed end of the specimen. The interface provides a high rate diffusion path for the environmental elements.

The characteristic diffusion coefficient of sulfur down the interface was estimated based on the diffusion problem for a semi-infinite solid ignoring curvature effects of the fiber. In this case, the solution will have the form:

$$S_s(z,t) = S_{s,\ \text{at } z=0}\ [1 - \text{erf}(z/2(Dt)^{\frac{1}{2}})] \qquad (2)$$

The diffusion distance of sulfur is defined as the distance from the end of the specimen to the location where the sulfur concentration drops to half the initial concentration.[2] From Fig. 2, the diffusion distance is, then, 140 μm from the end of the free surface.

Again, $C/C_s = [1 - \text{erf}(z/2(Dt)^{\frac{1}{2}})]$. Then $\text{erf}(z/2(Dt)^{\frac{1}{2}}) = 1$, Therefore, $z/2(Dt)^{\frac{1}{2}} = 0.477$, giving $z \approx (Dt)^{\frac{1}{2}}$. With $z = 140$ μm and $t = 4.3\times10^4$ sec, D is calculated 4.5×10^{-9} cm^2/sec at a maximum temperature of 550°C during thermal cycling for SiC/Ti-6Al-4V composite.

The oxygen diffusivity was also calculated, based on the same argument, to be 6.7×10^{-9} cm^2/sec for $B_4C/B/Ti\text{-}6Al\text{-}4V$ composite having z=170 μm. The bulk diffusion coefficient of oxygen in titanium is about 10^{-15} cm^2/sec.[3-5]

SEM fractography shows the presence of branch crack on the matrix side of the interface. The branch cracks extend an equivalent distance to the AES sulfur detection distance (Fig. 4). This implies that the interface cracking normal to the propagating main crack is associated with the thin but finite sulfide layer at the interface.

A.2 Two-dimensional diffusion analysis

In the last section, the diffusion phenomena was considered as a unidirectional flow of sulfur through the interface from the end of the specimen. The resultant expression of diffusion was the logarithm of sulfur concentration at the interface proportional to the diffusion distance measured from the end of the specimen. On the other hand, the sulfur diffuses into the titanium matrix bulk normal to the interface. Therefore, the problem is a two-dimensional diffusion of sulfur.

The interface is considered to be a thin layer of high diffusivity area between the titanium matrix and the fiber. The problem is to determine the concentration of solute in a semi-infinite solid having a semi-infinite slab as the interface of highly permeable material embedded in it. The analysis in the z-direction (along the interface) was made by getting Auger spectrum on several points

selected along the interface. The y-direction analysis was made by argon ion sputtering one of select points (at 150 μm from the end of the specimen) into the matrix.

The diffusion profiles of the solute from AES analysis indicate that the bulk diffusion is small compared to the diffusion on the interface (Figs. 5 and 1). The results of the sputtering by argon ion show that the sulfur diffused into the bulk only up to 4 nm for a one day thermal cycling. The solute diffuses up to 400 μm down the interface for the same period of thermal cycling, a 10^5 difference in diffusion distance. This confirms that the interface is in high energy state which provides high mobility of the environmental elements. Under these conditions, the grain boundary diffusion equation proposed by Fisher[6] can be applied to the present interface diffusion of sulfur in the environment in the titanium MMCs.

Consider the interface* to be a thin layer of high diffusivity area between the titanium a matrix and the B_4C/B fiber. The model system is shown in Fig. 6. The problem is to determine the concentration of sulfur in a semi-infinite solid having a semi-infinite slab as the interface of highly permeable material embedded in it.

The boundary conditions are:

$$C = C_s \text{ for } z=0 \text{ and } t \geq 0$$
$$C = 0 \text{ for } z > 0 \text{ at } t = 0 \qquad (3)$$

*The interface can be considered to be approximately a plane ignoring the curvature effects of the 150 μm fiber diameter.

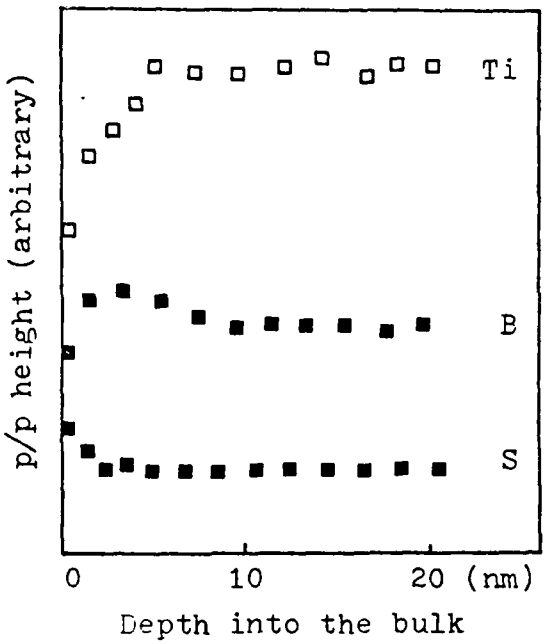

Figure 5. Depth profiles of B_4C/B/Ti-6Al-4V composite thermal cycled in S for one day, matrix side interface. True concentrations, $C_s(y)$, are obtained in Fig. 2 (in Appendix B).

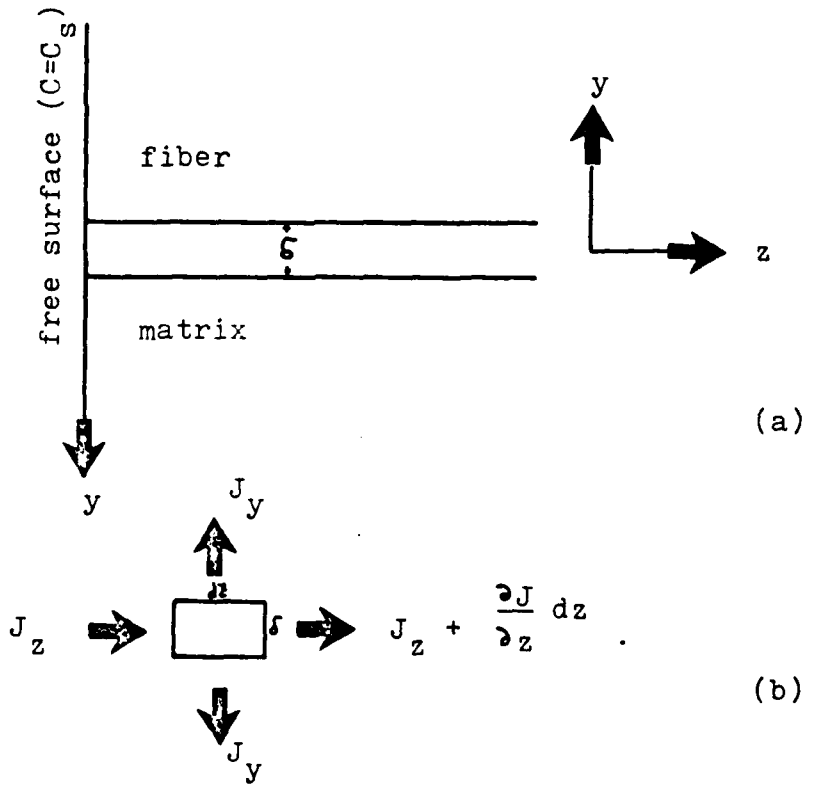

Figure 6. Schematic illustration of the geometry of the analysis. (δ the interface thickness)

Following Fisher's analysis[6], the differential equation which is valid inside the interface slab can be obtained. Consider an element of the slab which is dz long by δ thick by unit length deep. The fluxes into, or out of, the faces normal to the y and z axes are shown in Fig. 6b. Any plane normal to the x-axis is a symmetry plane, so J_x would be equal to zero. Then,

$$\begin{aligned} \partial C/\partial t &= (1/1dz\delta)(\delta(J_z - J_z - (\partial J_z/\partial z)dz) - 2dzJ_y) \\ \partial C/\partial t &= -\partial J_z/\partial z - (2/\delta)J_y \end{aligned} \tag{4}$$

J_y is the flux out of the interface into the bulk and can be replaced by $-D_b(\partial C/\partial y)$ with the gradient evaluated in the bulk just outside the interface slab. An expression for J_z can be obtained if an interface diffusion coefficient D_i is defined by the equation

$$J_z = -D_i \frac{\partial C}{\partial z} \tag{5}$$

Then,

$$\frac{\partial C}{\partial t} = D_i \frac{\partial^2 C}{\partial z^2} + \frac{2D_b}{\delta} \left(\frac{\partial C}{\partial y}\right)_{y=\frac{\delta}{2} \text{ or } y=0} \tag{6}$$

Outside the interface, diffusion would obey the equation

$$\frac{\partial C}{\partial t} = D_b \nabla^2 C = D \frac{\partial^2 C}{\partial y^2} \tag{7}$$

The approximate solution of eqs. 6 and 7 is obtained as follows based on several experimental observations. The interface concentrations, at some point, as measured after two different aging times were

within 20% difference during the thermal cycling treatment (Fig. 7). It was also observed that the diffusion of sulfur into the bulk was very slow.

It can then be assumed that the interface concentration, $C_b(y)$, is imposed on each slice at the slab not too far from the free surface and held constant for the duration of the heat treatment. It is also assumed that the flux of solute in the bulk is normal to the interface slab. Then the system can be replaced with a series of slices normal to the z-axis of thickness dz.

The concentration in each slice is then given by the equation,

$$C(y,z,t) = C_i(z)\,[1 - \mathrm{erf}(y/2(Dt)^{\frac{1}{2}})] \tag{8}$$

On integration by connecting the points of equal concentration in this "sliced" model,

$$C_i(z) = C_o \exp\left[\frac{-z\sqrt{2}}{(\pi D_b t)^{\frac{1}{4}}(\delta D_i/D_b)^{\frac{1}{2}}}\right]$$

Giving

$$C(y,z,t) = C_o \exp\left[\frac{-z\sqrt{2}}{(\pi D_b t)^{\frac{1}{4}}(\delta D_i/D_b)^{\frac{1}{2}}}\right]\left[1 - \mathrm{erf}\left(\frac{y}{2\sqrt{D_b t}}\right)\right] \tag{9}$$

Here, the amount of solute in each of a series of slices dz thick and parallel to the edge of the specimen will be

$$\bar{C}(z,t)dz = C_i(z)dz \int_{-\infty}^{\infty} \left[1-\mathrm{erf}\left(\frac{y}{2\sqrt{D_b t}}\right)\right] dy$$

$$= C_i(z)dz\ [\text{constant}] \tag{10}$$

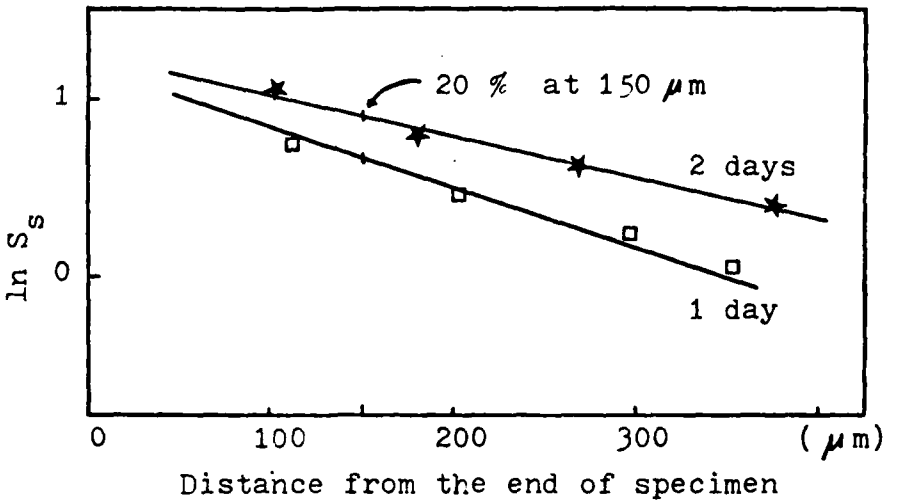

Figure 7. Logarithmic fitting of sulfur concentration along the interface showing the concentration difference for two different aging times is about 20%, for B_4C/B/Ti-6Al-4V thermal cycled in sulfur to 540°C.

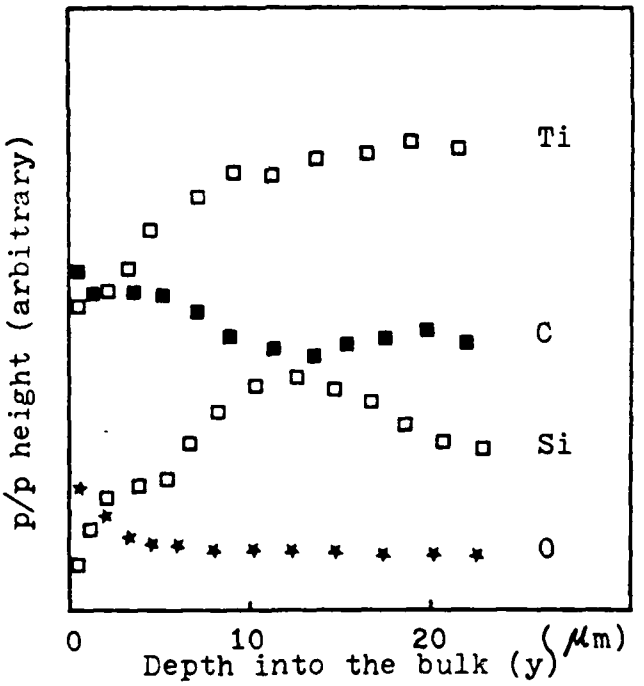

Figure 8. Depth profiles of SiC/Ti-6Al-4V composites thermal cycled in air, matrix side of interface.

A plot of ln $\bar{C}$ vs z then should give a straight line of slope,

$$\frac{-\sqrt{2}}{(\pi D_b t)^{\frac{1}{4}}(\delta D_i/D_b)^{\frac{1}{2}}}$$

This diffusion analysis conforms to the experimental results giving a straight line fitting of ln $\bar{C}$ vs z (Fig. 7). From this relationship, the bulk diffusion coefficient of sulfur was calculated to be 1×10^{-20} cm^2/sec and that of oxygen was 2×10^{-20} cm^2/sec. The bulk diffusion of sulfur measured from Fig. 2 in Appendix B gave the diffusivity of 2×10^{-19} cm^2/sec. These values are different from those in the literature[3-5], where the diffusion of oxygen was in α-titanium. In this study, the interface consists of various complex titanium compounds which will change the movement of oxygen.

The activation energies, E_a, for the diffusion along the interface during thermal cycling were about 15 Kcal/mole for sulfur and 8 Kcal/mole for oxygen respectively. It is reported[9] that E_a for the sulfurization reaction of titanium is about 27 Kcal/mole; that of sulfur segregation in powdered titanium is 15.5 Kcal/mole in the temperature range of 25 to 700°C[10].

The analysis indicated that the sulfur concentration decreases exponentially with the diffusion distance, ln $C_s = k'z$. As discussed previously, k' is the proportionality constant. The rapid diffusion down the interface was separated from the slow diffusion into the bulk resulting in two one-dimensional analyses. The sulfur has negligible solubility in titanium of about 0.017 w/o.[7] Sulfur forms eleven different sulfides in the phase diagram (Table 1)[8], which

results in the sputtering profiles, Fig. 5, showing continuously decreasing sulfur content into the bulk. A plateau in the sulfur profile would be observed if thicker single concentration sulfides existed in the interface layer, an observation made recently for measurements close to the end of the specimen. The actual diffusion coefficient is for sulfur diffusing through a series of closely related Ti_xS_y structures. The same expression is applicable for the oxygen diffusion since the oxygen diffusion into the bulk is also slow. Oxygen was removed after 3 min of sputtering corresponding to about 6 nm in depth for the specimen thermal cycled for one day (Figs. 3 and 8).

Additional measurements as a function of temperature and time are presently being made to extend the diffusion analysis.

Table 1

Summary of Phases in the S-Ti System[8]

Designation	Composition		Parameters, A
	S/Ti	(a/o S)	
TiS_3	3.0	(75)	a = 4.973, b = 3.433, c = 8.714, β = 97 74°
TiS_2-Ti_2S_3			
TiS_2	1.919–1.810	(65.74–64.41)	a = 3.4085–3.4131, c = 5.7028–5.7176
Ti_2S_3	1.810–1.594	(64.41–61.45)	
Ti_2S_3	1.594–1.377	(61.45–57.93)	a = 3.4219–3.4422, c = 11.4419–11.4298
Ti_2S_3-TiS			
Ti_3S_4	1.30_5–1.28_3	(56.61–56.20)	a = 5.98 ± 0.01, b = 3.440 ± 0.006, c = 10.14 ± 0.02, β = 95°40′ ± 20′
Ti_4S_5	~1.25	(~55.6)	
$Ti_{1-x}S$	1.20_4–1.13_3	(54.63–53.12)	a = 3.4245 ± 0.0001, c = 26.493 ± 0.001
TiS	1.06_5–~0.97	(51.46–49.24)	a = 3.2988 ± 0.0002, c = 6.3796 ± 0.0004
Subsulfides			
TiS_{1-x}	. . .	(~40)	a = 3.272 ± 0.002, c = 6.440 ± 0.004
TiS_{1-y}	. . .	(~40)	a = 3.2873 ± 0.0002, c = 3.2105 ± 0.0002
Ti_6S	. . .	(~14)	a = 2.9669 ± 0.0004, c = 14.495 ± 0.005

References

1. Handbook of Auger Electron Spectroscopy, Physical Electronics, Inc., 2nd edition, 1976.

2. L.S. Darken and R.W. Gurry in Physical Chemistry of Metals, 1953, p. 444.

3. Y.A. Bertin, et al., in Titanium '80 (H. Kimura, ed.), AIME, 1980, p. 530.

4. M. Dechamps and P. Lehr, J. Less Common Metals, vol. 56, 1977, p. 193.

5. D. David, et al. J. Less Common Metals, vol. 65, 1979, p. 51.

6. J.C. Fisher, J. Appl. Physics, vol. 22, 1951, p. 74.

7. L.B. Berger, et al., TMS-ASM, vol. 49, 1957, p. 300.

8. S.A. Shunk in Constitution of Binary Alloys, 2nd supplement, McGraw-Hill Book Co., 1969.

9. J.E. Dutrizac, J. Less Common Metals, vol. 51, 1977, p. 283.

10. C.P. Lofton and W.E. Swartz, Jr., Appl. Spectroscopy, vol. 32, 1978, p. 177.

Appendix B

Correction of Concentration Profiles from AES Peak-to-Peak Height Measurements

Conventionally, the relative peak-to-peak (p/p) height of the element of a depth y below the top surface after sputtering are converted to composition using a relative sensitivity factor from the AES Handbook.[1]

When the elemental standards are used, the intensity ratios from the standards must be corrected by factors related to the atom density, electronic escape depth and electron back scatter factor. This improves the accuracy with which the Auger peak intensities can be related to the surface composition.[2] However, the surface composition may still not equal the bulk composition. Several attempts[2-8] have been published to quantify the AES data for the distribution of elements on the surface. Even though the effect of escape depth was emphasized, no one used it directly for the quantitative surface analysis of the material with thin layer structure.

In the present problem, since sulfur is present as a thin layer on the interface, the concentration of sulfur will be different from the conventional calculation approaches which assume bulk concentration.

The p/p height of sulfur, S(y), measured at a depth of y after sputtering is proportional to

$$\int_y^\infty C_s(\xi) e^{-(\xi-y)/\delta} d\xi \qquad (1)$$

where $C_s(\xi)$ is the true concentration at a depth of ξ from the sputtered surface and δ is the escape depth, as shown in Fig. 1. The data is taken at a specific value of z, the distance down the boundary from the free surface.

Now, the problem is to get $C_s(y)$ from the following integral equation: From equation 1 with a change in variable,

$$S(y) = N\int_0^\infty C_s(\xi+y)e^{-\xi/\delta}d\xi \tag{2}$$

where N is the sensitivity of the element excluding the escape depth. In a derivation by H.A. Stevens[9], eq. 2 can be rewritten as follows in terms of $C_s(y)$. Since

$$\begin{aligned}\frac{dS(y)}{dy} &= N\int_0^\infty d\xi\,\frac{d}{dy}\,C_s(\xi+y)e^{-\xi/\delta}\\ &= N\int_0^\infty d\xi\,\frac{d}{d\xi}\,C_s(\xi+y)e^{-\xi/\delta}\\ &= N\left[C_s(\xi+y)e^{-\xi/\delta}\Big|_{\xi=0}^{\xi=\infty} + \frac{1}{\delta}\int_0^\infty d\xi C_s(\xi+y)e^{-\xi/\delta}\right]\\ &= -NC_s(y) + \frac{1}{\delta}\,s(y)\end{aligned} \tag{3}$$

Then,

$$C_s(y) = \frac{1}{N}\left[\frac{S(y)}{\delta} - \frac{dS(y)}{dy}\right] \tag{4}$$

This gives the true surface chemistry in terms of the measured value and the slope of the inert ion sputtering profile. The experimental sulfur profile results can be curve-fit in the form shown in Fig. 1.

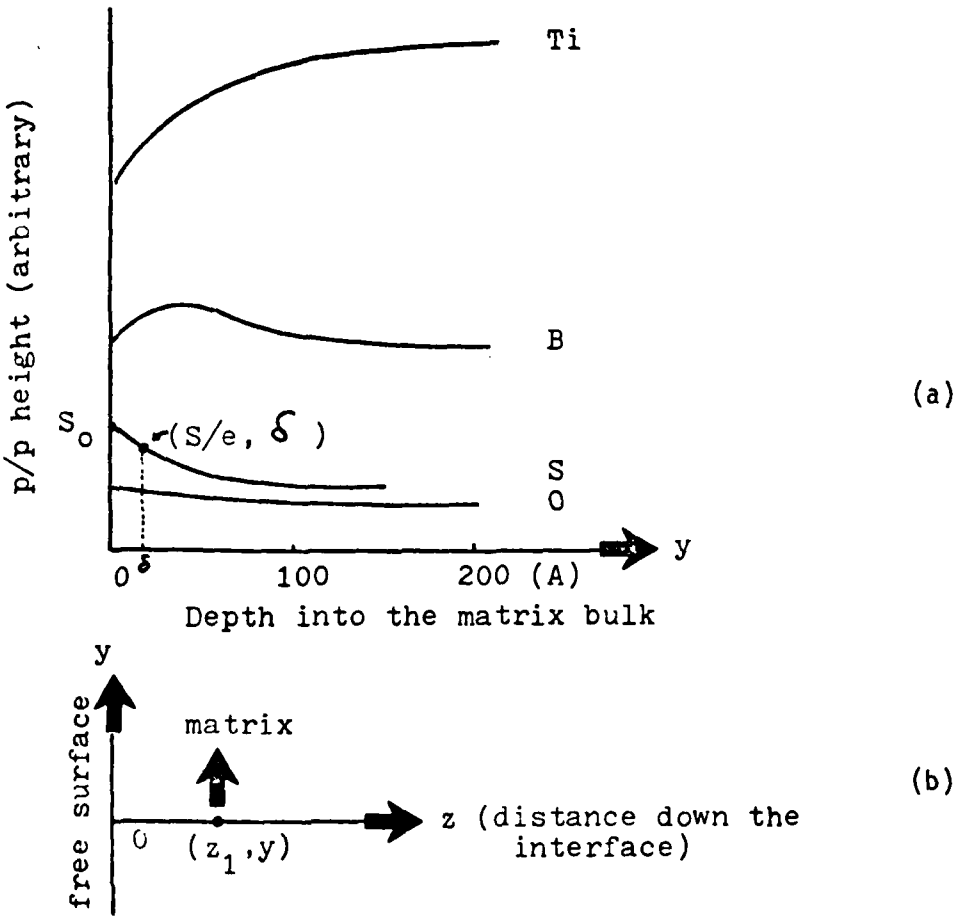

Figure 1. Sputtering depth profile (from Fig. 5 in Appendix A) and the geometry of the analysis. (δ the escape depth)

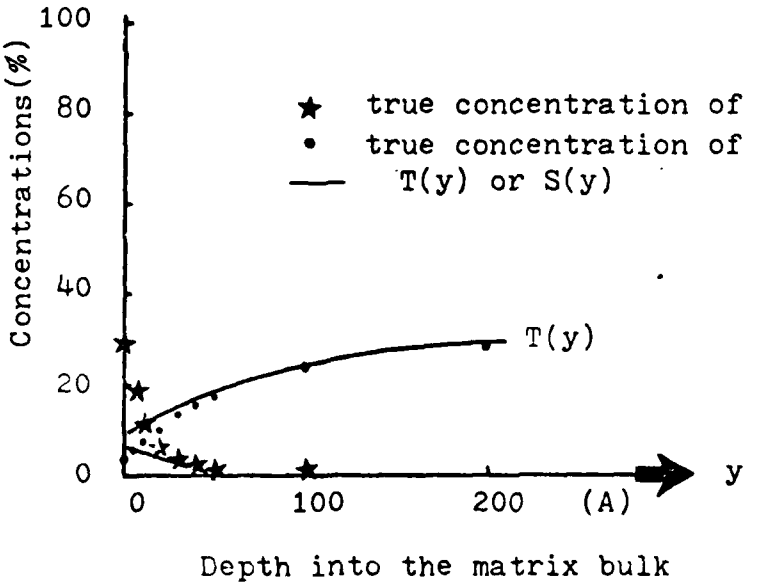

Figure 2. Diagram of true concentrations of sulfur, $C_s(y)$ and Ti, $C_{Ti}(y)$.

$$S(y) = S_o e^{-\alpha y} \tag{5}$$

S_o is the p/p height at y=0. Since

$$\frac{dS(y)}{dy} = -\alpha S_o e^{-\alpha y} \tag{6}$$

Eq. 4 can be rewritten

$$C_s(y) = \frac{S_o}{N}\left[\frac{1}{\delta} + \alpha\right] e^{-\alpha y} \tag{7}$$

From Fig. 1, the value of y where the p/p height of sulfur equals S_o/e is found to be 13 Å. From this observation,

$$S(y)\big|_{y=13} = S_o e^{-\alpha \cdot 13} = \frac{S_o}{e}$$

giving $\alpha = 0.077$ Å^{-1}.

With the δ of the sulfur being 8 Å,

$$C_s(y) = \frac{S_o}{N}\left[\frac{1}{8} + 0.077\right] e^{-0.077y}$$

$$= 0.202 \frac{S_o}{N} e^{-0.077y} \tag{8}$$

$$S(y) = S_o e^{-0.077y} \tag{9}$$

Here S_o/N cannot be obtained by observing the sulfur profile alone. Observation of the titanium sputtering profile, T(y), can allow the determination of the true titanium concentration, $C_{Ti}(y)$. The sputtering profiles of boron and others including carbon, aluminum and vanadium are found to be approximately constant, giving C_B=55%, C_{others}=15%;

since below the depth of at least 3δ, the concentrations calculated based on AES Handbook will give approximately true concentrations of elements such as titanium, boron, carbon, aluminum and vanadium, and their sum should be 100%.

From the experimental observations, the p/p height of titanium is given by

$$T(y) = 0.3(1-pe^{-\beta y}) \tag{10}$$

since $T(y) \to 0.3$ as $y \to \infty$ (considering C_B=0.55 and C_{others}=0.15). Similarly,

$$T(y) = M \int_0^\infty C_{Ti}(\xi+y)e^{-\xi/\delta}d\xi \tag{11}$$

where M is the sensitivity of the titanium and δ_{Ti}=12 Å. At y=20 Å, $T(y)_{at\ y=20} = 0.3\ (1-pe^{-20\beta}) = \frac{1}{2} \times 0.3$ and y = 40 Å, $T(y)_{at\ y=40} = 0.3\ (1-pe^{-40\beta}) = 2/3 \times 0.3$. Then, β=0.002 and p=0.75.

Therefore,

$$C_{Ti}(y) = \frac{1}{M}\left[\frac{1}{\delta} - pe^{-\beta y}\left(\frac{1}{\delta} + \beta\right)\right]$$

$$= \frac{1}{M}\left[0.083-(0.75)(0.103)e^{-0.02y}\right]$$

$$= \frac{1}{M}\left[0.083-0.078e^{-0.02y}\right]$$

Again since, as $y \to \infty$, $C_{Ti} \to 0.3$, M = 0.277. Therefore,

$$C_{Ti}(y) = 0.30 - 0.282e^{-0.02y} \tag{12}$$

$$T(y) = 0.30 - 0.225e^{-0.02y} \tag{13}$$

From the mass conservation, $C_{others} + C_B + C_{Ti} + C_s = 1$ at y=0. Then,

$$C_s = 0.282 = \frac{S_o}{N}(0.202)e^{-0.077 \cdot 0}. \qquad \frac{S_o}{N} = 1.4.$$

Therefore,

$$S(y) = S_o e^{-0.077y} \tag{14}$$

$$C_s(y) = 0.282e^{-0.077y} \tag{15}$$

In summary, the results are shown in Table 1 and in Fig. 2.

As shown above, S(y) or T(y) should be corrected to $C_s(y)$ or $C_{Ti}(y)$ to obtain true concentrations of the elements. In the course of these derivations, several variables were not taken into account. These include, (1) preferential sputtering effects, (2) surface roughness, (3) interaction effects between elements, (4) knock-in effects, and (5) peak shape changes (not too significant for sulfur and titanium).

Even with the other variables not taken into account this attempt to quantify the thin layer chemistry offers a much more meaningful approach. In particular, where the absolute surface concentrations are required for a diffusion analysis, the approach is even more useful. Present studies are obtaining sufficient data to do the complete two-dimensional analysis for the Ti-MMC.

Table 1

Calculated concentrations* of the elements

y (Å)	C_B	C_{others}	$C_{Ti}(y)$	T(y)	$C_s(y)$	S(y)**	Total
0	0.55	0.15	0.02	0.08	0.28	0.05	1.00
5	0.55	0.15	0.05	0.10	0.19	0.03	0.94
10	0.55	0.15	0.07	0.12	0.13	0.02	0.90
20	0.55	0.15	0.11	0.15	0.06	0.01	0.87
30	0.55	0.15	0.14	0.18	0.03	0.004	0.87
40	0.55	0.15	0.17	0.20	0.01	0.001	0.88
50	0.55	0.15	0.20	0.22	0.00	0.00	0.90
100	0.55	0.15	0.27	0.27	0.00	0.00	0.97
200	0.55	0.15	0.29	0.30	0.00	0.00	0.99

*Concentrations are in atomic fractions.

**Obtained from the p/p height method.

References

1. Handbook of Auger Electron Spectroscopy, Physical Electronics, Inc., 2nd edition, 1976.

2. P.H. Holloway and S.K. Hofmeister, Surf. Interf. Analysis, vol. 4, 1982, p. 181.

3. J.F. Smith and H.N. Southworth, Surf. Sci., vol. 122, 1982, p. L619.

4. J. Cazaux, J. Microsco. Spec. Electro., vol. 7, 1982, p. 487.

5. S. Bouquet et al., Spec. Electro., vol. 7, 1982, p. 447.

6. G. Luckman, L.A. Adler and W.R. Graham, Surf. Sci., vol. 121, 1982, p. 61.

7. L.V. Phillips, et al., ASTM-STP 643, 1978, p. 47.

8. L. Marchut and C.J. McMahon, in Electron and Positron Spectroscopies in Materials Science and Engineering, 1979, Academic Press, p. 183.

9. H.A. Stevens, private communication.

Appendix C

Fatigue Crack Growth Behavior of SiC and B_4C/B Reinforced Titanium Metal Matrix Composites

Introduction

Fatigue crack growth (FCG) behavior of SiC and B_4C/B reinforced titanium metal matrix composites loaded in the transverse direction was studied as a function of interface modifications and gaseous environments. This was investigated to determine if the change in interface chemistry and strength, which were modified by the diffusion of sulfur during thermal cycling, resulted in a change in the FCG behavior. Also studied was the effect of various gaseous environments such as humid lab air, dry nitrogen and dry hydrogen on the FCG rate. The heat treatment employed consisted of thermal cycling the composite specimens between RT and 550°C for 84 hours in an environment of sulfur.

C.1. Experimental

All FCP testing was performed on transverse specimens. Edge notched specimens with $a_o/w = 0.25$ and w=25 mm were used.* Aluminum doublers were glued at the ends using an epoxy glue to prevent load point failure. Fatigue cycling was performed on an MTS closed loop electrohydraulic system in the tension-tension mode, between 20 lb and 200 lb at a frequency of 2 Hz. Fatigue crack growth was monitored visually with the aid of several equidistant vertical lines normal to the notch inscribed on the specimen surface.

*a_o is the notch length and w is specimen width.

The first set of experiments was performed on both as-received and heat treated transverse specimens in laboratory air of approximately 50% R.H. In addition, to study the effects of gaseous environments on the FCP, experiments were also performed in atmospheres of dry nitrogen and dry hydrogen. For this purpose, a high vacuum system (sorption and ion pumps) connected to an environment chamber was employed. The vacuum pressure was measured by an ionization gauge and an ion pump gauge mounted on the chamber. The chamber was evacuated to 4×10^{-6} torr and the gases leaked in through a leak valve.

Finally, all the fatigue fractured surfaces were viewed in a JEOL 35 high resolution SEM to determine the failure paths and mechanisms and the effects of interface modification and gaseous environments on the failure mode. Multiple specimens were run in each set of experiments to permit duplication of results.

C.2. FCG for SiC/Ti-6Al-4V Composites

As mentioned earlier, the first set of experiments was carried out on both as-received and thermal cycled SiC/Ti(6Al-4V) specimens in laboratory air of 50% R.H. From visual monitoring of the crack propagation, a plot of da/dN vs. ΔK was obtained in each case. It was observed that the rate of crack growth in the heat treated specimens exceeded that of the as-received specimens slightly, indicating that the thermal cycling in S may be instrumental in degrading the fatigue resistance. Fractography on the as-received specimen indicated the presence of both fiber splitting and interfacial debonding

while the heat treated specimens showed only interfacial debonding (Figs. 1 and 2). These observed fracture modes are in agreement with Mahulikar's[1] results for BORSIC/Ti(6Al-4V) composites, where he noticed a transition from fiber splitting for the as-received condition to interfacial splitting for the heat treated condition. This fiber splitting seen in the case of FCP in humid air at R=0.1 was considered by him to be a result of the combination of humid air weakening of the fibers and an environmentally induced fatigue crack closure effect. At the load ratio in question, a significant amount of fatigue crack closure has been observed in isotropic materials. Fatigue crack closure is a result of the residual plastic deformation left in the wake of an advancing crack tip. This closure effect can set up stress fields on the fiber. Also, since the specimens are very thin, mode III stresses can be expected to act on the fibers during the lower part of the fatigue cycle during closure. In addition, in humid air, an oxide layer builds up on the crack surface and this gives rise to a higher value of the residual displacements for humid air than in the case of a vacuum. Since the humidity increases the crack closure load by oxide formation, these increased closure loads could also be responsible for the fiber splitting seen in humid air. This area, however, is not completely understood at present.

The next set of experiments was performed in dry N_2. Both the as-received and thermal cycled specimens showed considerably lower FCP rates in N_2 than in humid air although there was no conclusive difference in the FCP rates of the two sets of specimens in N_2.

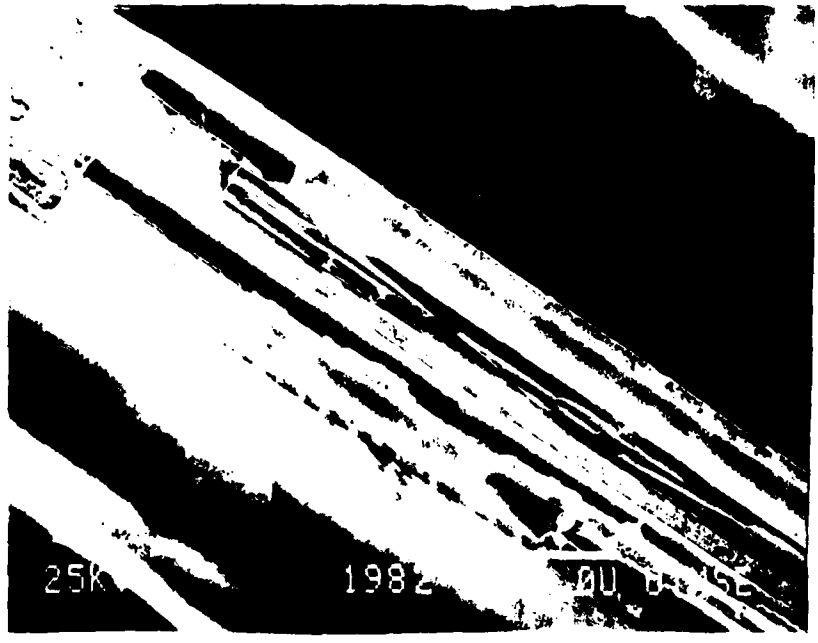

Figure 1. FCP in lab air for as-received SiC/Ti(6Al-4V)

Figure 2. FCP in lab air for thermal cycled SiC/Ti(6Al-4V)

Fiber splitting was seen on both fracture surfaces which is in contrast to Mahulikar's results for BORSIC, where fiber splitting occurred only in humid air (Figs. 3 and 4). This difference was attributed to better fiber matrix bonding in the SiC composites or to the increased brittleness of SiC fibers causing them to split in preference to debonding from the matrix.

The third set of experiments was carried out in dry H_2. The FCP rates for both the as-received and heat treated specimens were intermediate between the observed rates for dry N_2 and humid air. Again, however, the propagation rates for the two different specimens did not lie sufficiently far apart to permit any definite conclusions, although the rates for the heat treated specimens did exceed those of the as-received (Fig. 6). Fractography revealed the presence of fiber splitting and interfacial splitting in both cases (Fig. 5). Observed failure modes are summarized in Table 1.

C.3. FCG for B_4C/B/Ti-6Al-4V Composites Thermal Cycled in Sulfur

Figure 7 shows the results for the FCG tests in a transverse direction for as-received B_4C/B/Ti-6Al-4V specimens and then cyclically loaded at a load ratio, R=0.1, in approximately 50% RH air. FCG data for the annealed Ti-6Al-4V alloy in humid air and the results from Mahulikar[1] are also included for comparison. It was reported[2] that the fatigue crack growth results conducted on the Ti-6Al-4V alloy in humid air and inert dry argon at room temperature yielded almost identical cyclic crack growth rates. When the data

Figure 3. FCP in dry N_2 for as-received SiC/Ti(6Al-4V)

Figure 4. FCP in dry N_2 for thermal cycled SiC/Ti(6Al-4V)

Figure 5. FCP in dry H_2 for as-received SiC/Ti(6Al-4V)

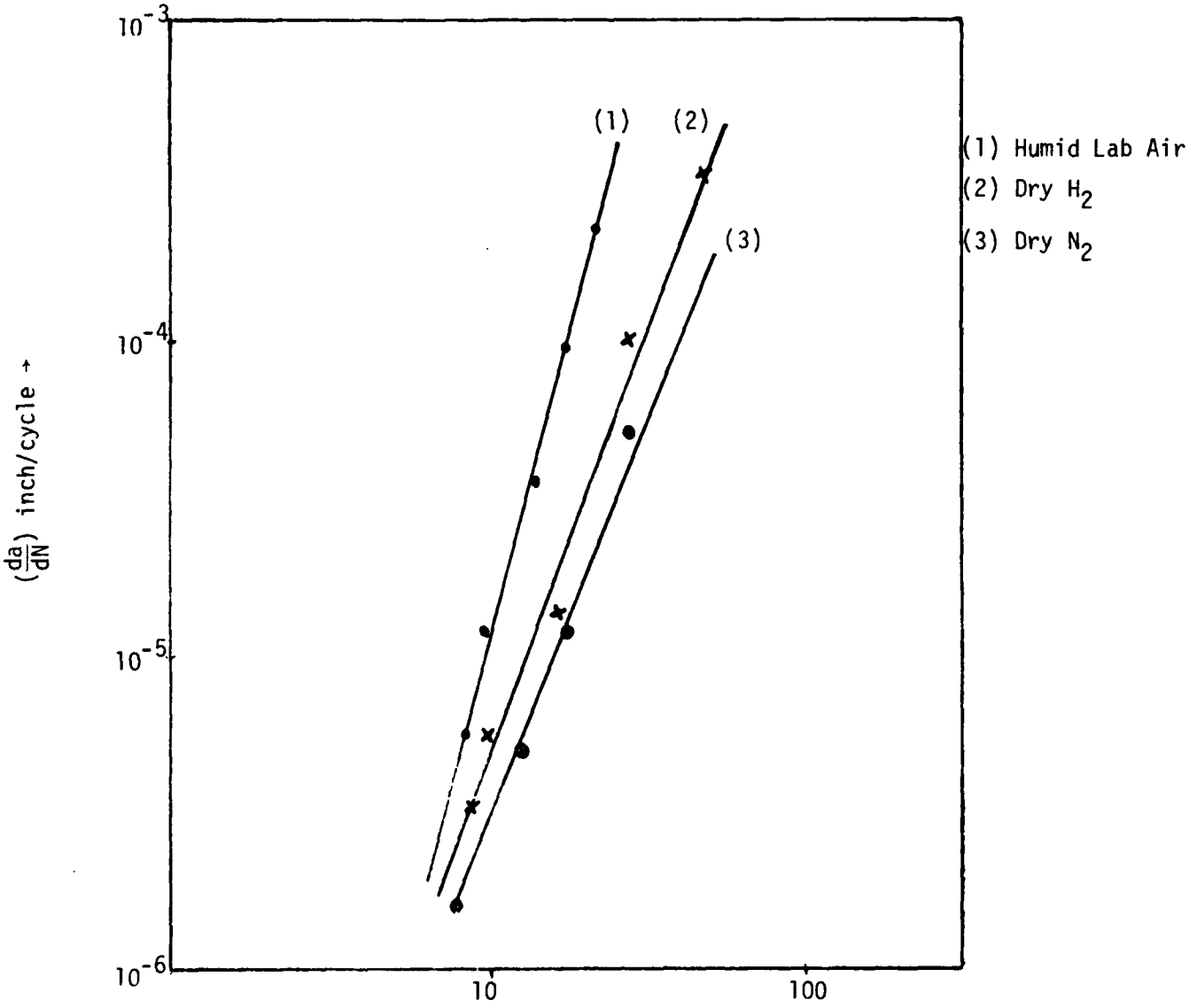

Figure 6a. FCP of as-received transverse SiC/Ti(6Al-4V) specimens in various gaseous environments.

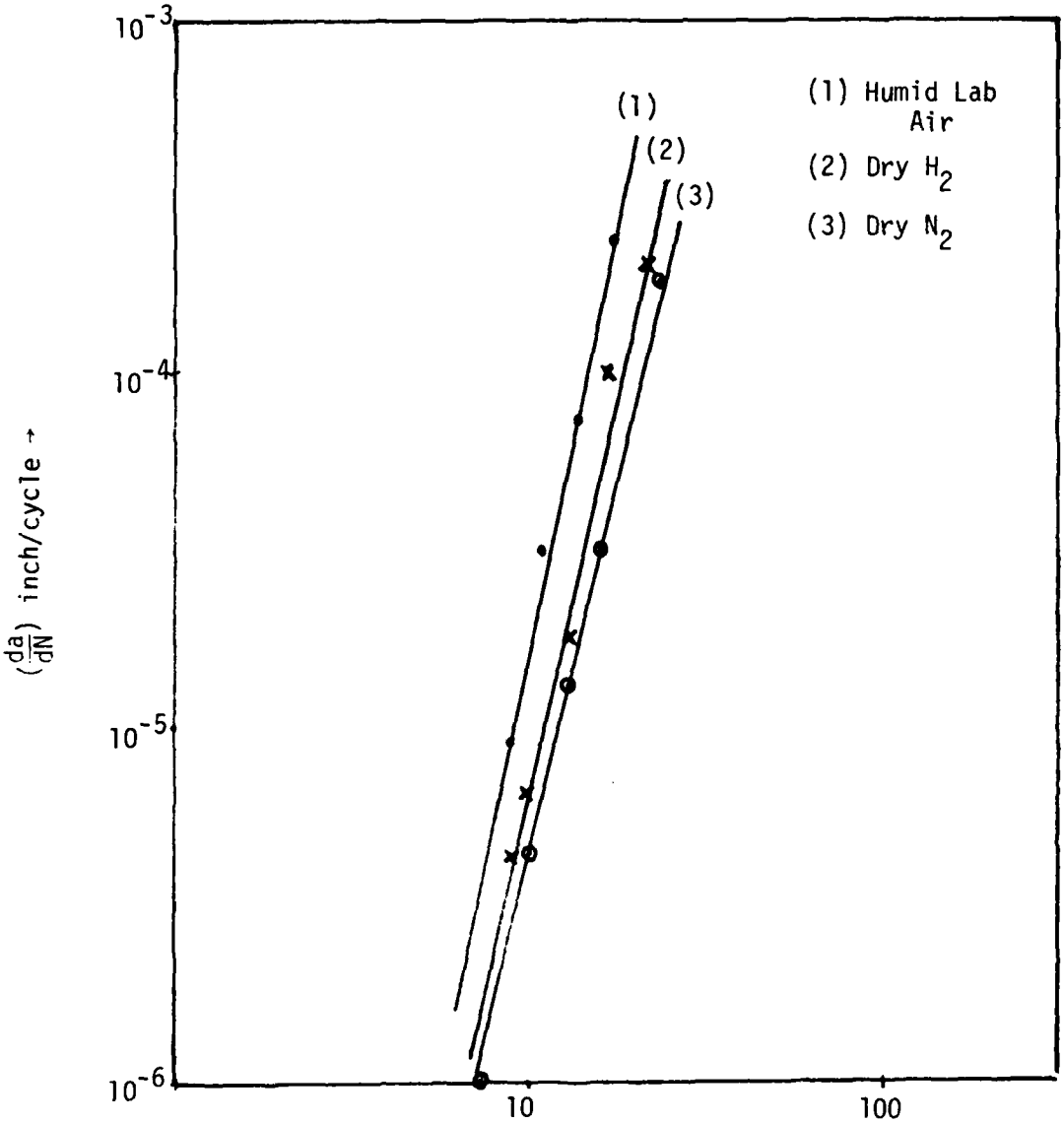

Figure 6b. FCP of thermal cycled transverse SiC/Ti(6Al-4V) specimens in various environments.

Table 1

Observed Failure Modes for the SiC/Ti(6Al-4V)

	AS-RECEIVED	THERMAL CYCLED IN S, 84 HRS at 550°C
LAB AIR (~50% R.H.)	FIBER SPLITTING/ INTERFACIAL SPLITTING	INTERFACIAL SPLITTING
DRY N_2	FIBER SPLITTING/ INTERFACIAL SPLITTING	FIBER SPLITTING/ INTERFACIAL SPLITTING
DRY H_2	FIBER SPLITTING/ INTERFACIAL SPLITTING	FIBER SPLITTING/ INTERFACIAL SPLITTING

are presented in a da/dN vs. ΔK plot, as shown in Fig. 7, it is clear that the stage II FCG of the composites along with a Ti-6Al-4V alloy can be expressed by Paris' law

$$da/dN \propto \Delta K^m$$

The slope (m) is identical for the Ti-6Al-4V alloy and the composites tested in the transverse direction. The results for composites show little difference in FCG between this study and Mahulikar's.

It is apparent that the FCG rates tend to be higher in humid environments. The fractography, shown in Fig. 8, indicate that the FCG in humid air was by an increased amount of fiber splitting as reported here and from Mahulikar.[1] The FCG in dry N_2 environment, on the other hand, was more often by interface debonding with some of fiber splitting and fiber fracture (Fig. 9). Mahulikar observed predominant interfacial debonding for the as-received specimen for FCG in N_2.

A second set of FCG experiments was carried out for the specimens thermal cycled in sulfur. The result is shown in Fig. 10. Specimens thermal cycled in sulfur show higher FCG rates in lab air than the as-received sulfur free specimens. The slope (m) is greater for those specimens. When sulfur is at the interface following thermal cycling in the sulfur environment, the FCG rate in humid air increases and is accompanied by interface debonding. SEM fractography in Fig. 11 shows well-defined interface debonding.

The FCG results for the samples thermal cycled in a sulfur environment and tested in dry N_2 gas indicated a slight decrease but

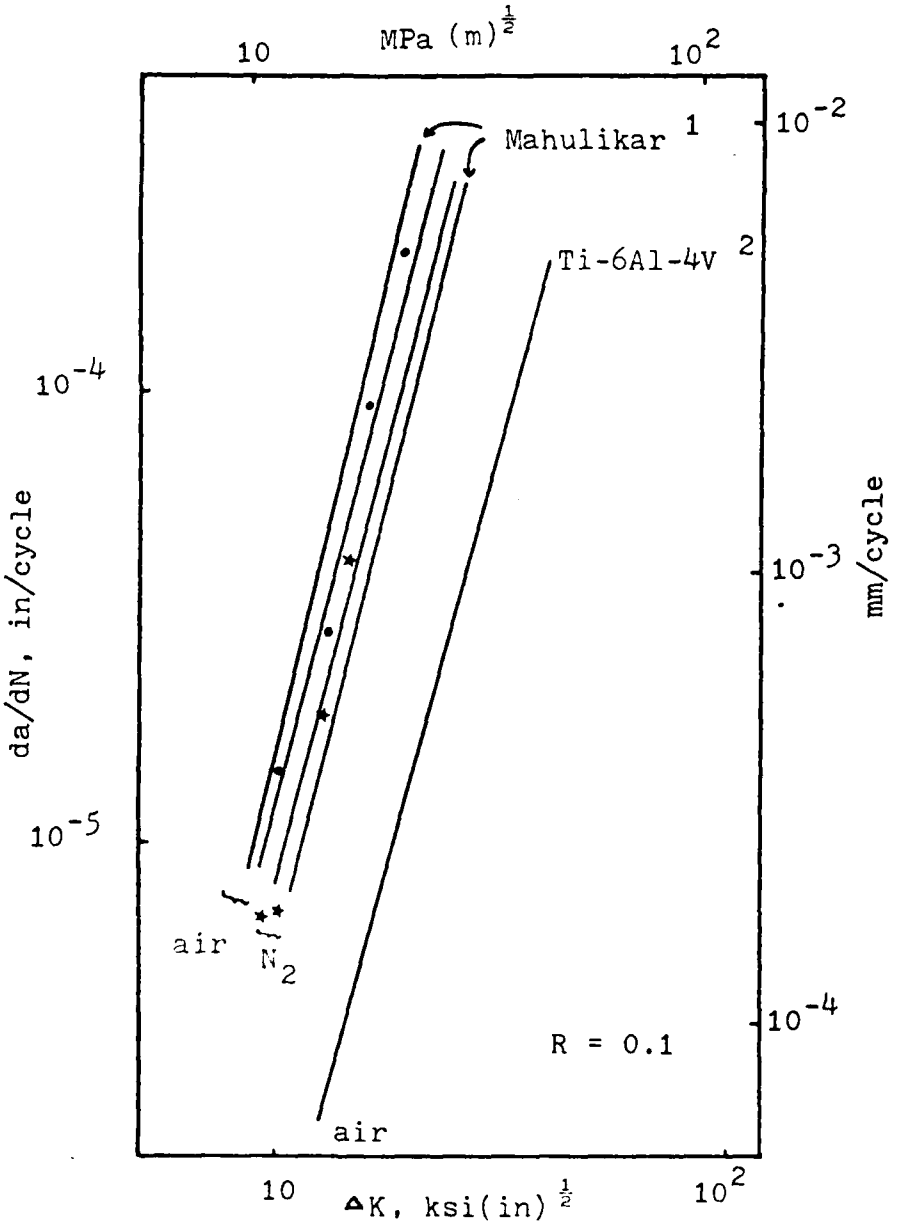

Figure 7. FCG rates for as-received B_4C/B/Ti-6Al-4V composites from this study and Mahulikar[1] as well as annealed Ti-6Al-4V sheet.

Figure 8. SEM fractograph of FCG in air for as-received B_4C/B/Ti-6Al-4V, transverse.

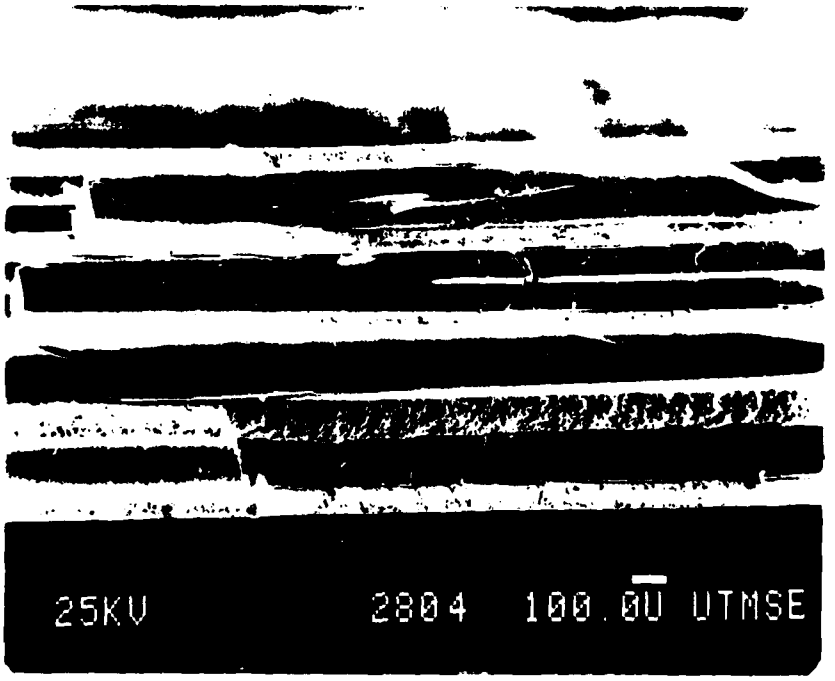

Figure 9. SEM fractograph of FCG in dry N_2 for as-received B_4C/B/Ti-6Al-4V, transverse.

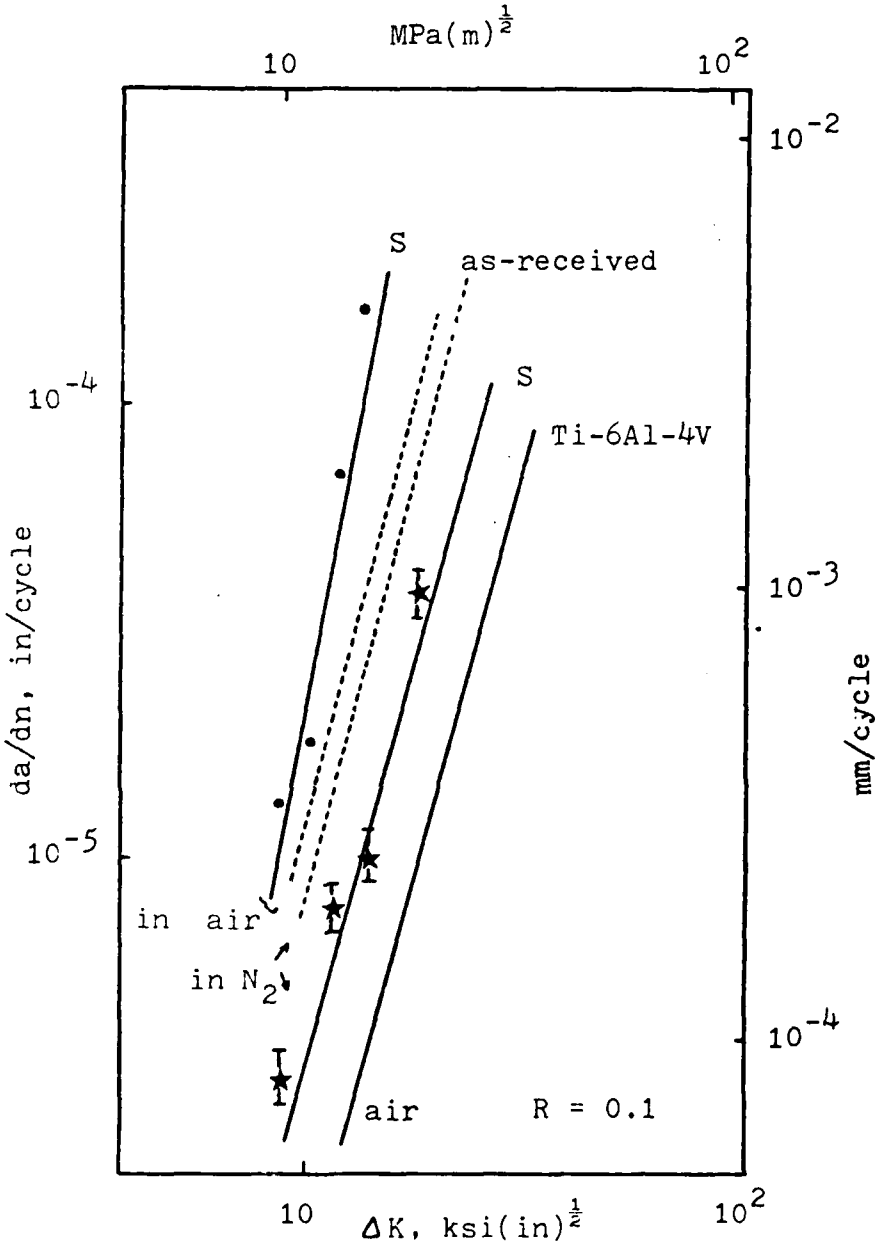

Figure 10. FCG rates for B_4C/B/Ti-6Al-4V thermal cycled in sulfur, transverse.

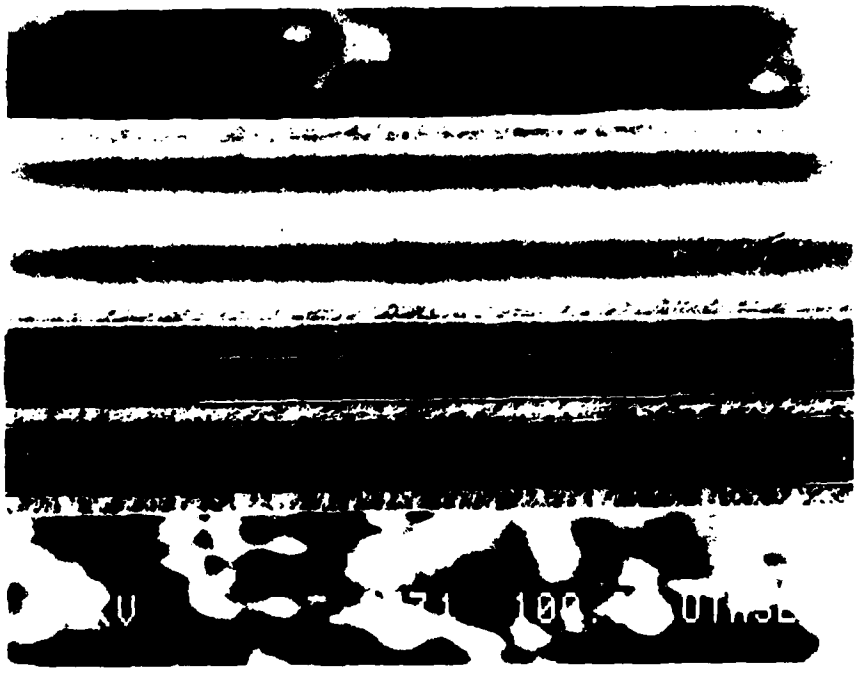

Figure 11. SEM fractograph of FCG in air for B_4C/B/ Ti-6Al-4V thermal cycled in sulfur, transverse.

a large scatter in growth rate with the same slope as the dry N_2 FCG rates of the as-received specimens. The FCG in air of SiC/Ti-6Al-4V composites thermal cycled in sulfur showed an enhanced crack growth as is reported here for the case of B_4C/B/Ti-6Al-4V composites. The fractography of N_2 tested sulfur enriched B_4C/B/Ti-6Al-4V composite, shown in Fig. 12, shows fracture modes such as fiber splitting, fiber fracture and matrix fracture similar to those for FCG in N_2 of as-received specimens. This similar fracture mode would explain the similar value of m with the as-received specimen.

The presence of the interface in the titanium MMCs change the da/dN vs. $\Delta K/E$ plot. When the ΔK is normalized to account for the elastic modulus of the respective materials [$E_{composite}$=140 GPa (20×10^6 psi), E_{Ti}=116 GPa (16.8×10^6 psi)] to have comparable crack opening displacement $(COD)^3$, the composite FCG is still greater than that of Ti-6Al-4V matrix with the slopes (m) virtually unchanged, as shown in Fig. 13. The fiber directions along the interface or through split fibers are the least resistant path for the transverse FCG. The FCG in the composite is self-similar, i.e., along the notch direction which was made along the fiber direction. With the exceptions of the enriched sulfur tested in humid air the fracture strength is dominated by the crack growth resistance of the titanium matrix. This is indicated by the fact that the slopes (m) of the da/dN vs. $\Delta K/E$ plots are the same, although the rates of crack growth in the composites are significantly higher than for the

Figure 12. SEM fractographs of FCG in dry N_2 for B_4C/B/ Ti-6Al-4V thermal cycled in sulfur, transverse.

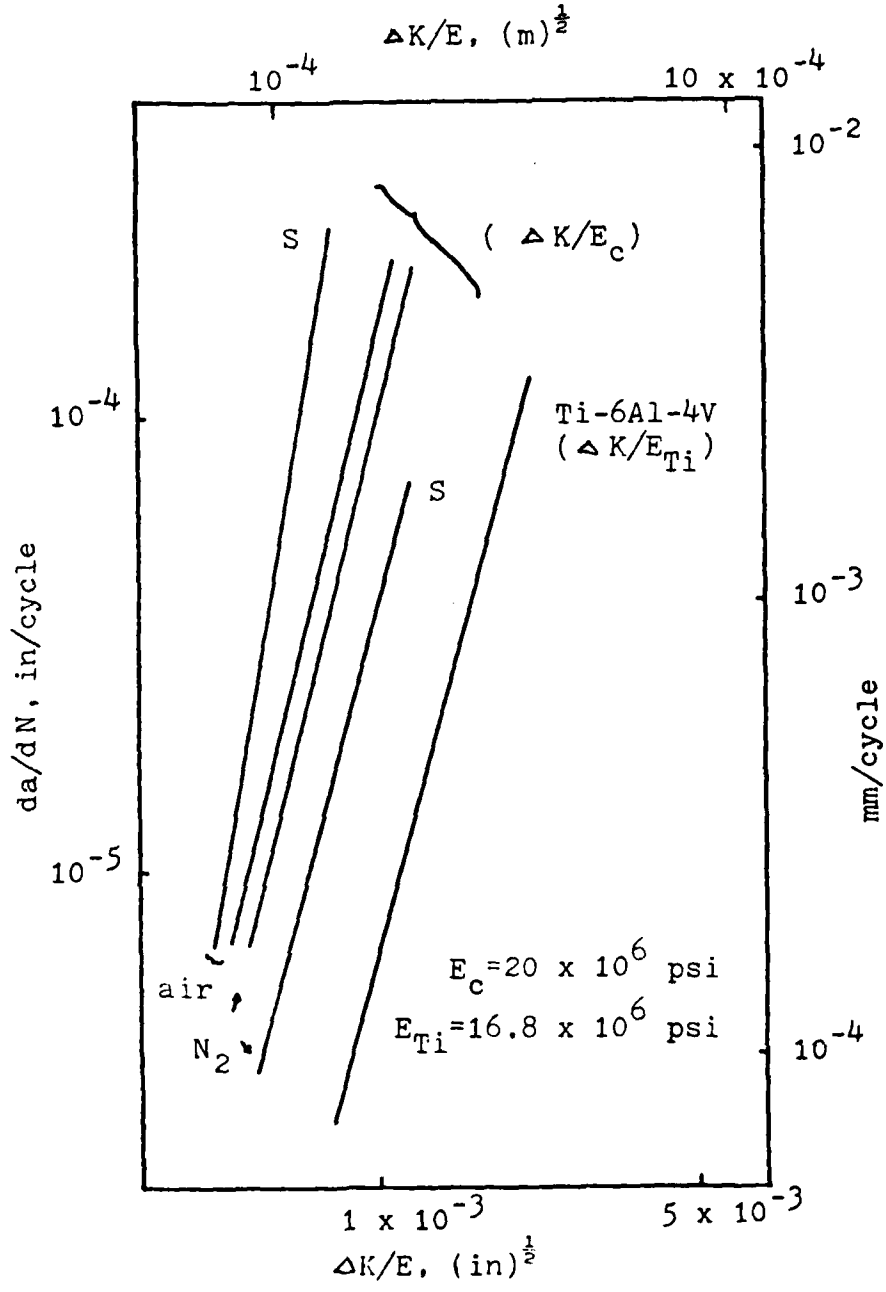

Figure 13. FCG rates after the normalization of ΔK by the elastic modulus, for B_4C/B/Ti-6Al-4V composite.

titanium alloy. This can be explained by the brittle fiber fracture not carrying its share of the stress. In fact if it is assumed that all the cyclic stress and COD are accommodated by the matrix material the equivalent $\Delta K/E$ would translate the results to match the Ti-6Al-4V results (Fig. 14). The amount of translation of ΔK_{tr} will be 1.7 $\Delta K_{composite}$ since the load is carried by matrix with a volume fraction of 60% for the transverse specimen.

The sulfur enriched interface of the specimen thermal cycled in sulfur reacts with the humidity in the air during FCG in lab air to degrade the interface cohesion resulting in complete separation of the interface from the matrix and the fiber at low strains. This total inability of the interface to sustain any strain further increases the fatigue crack growth rate in the matrix. The increase in the value of the slope may be due to the degradation of the interface by titanium sulfides creating a volume of brittle materials. This then leads to interface debonding.

The results presented here demonstrate that the interface between the matrix and fiber does transfer load during fatigue cycling in either an inert environment or if the interface has a minimal amount of impurities.

On the basis of the results of the experiments described above, a model for the failure mechanism for the FCG of the transverse titanium MMCs can be proposed. The model is schematically shown in Fig. 15. Only the matrix deforms plastically. Due to the high degree of anisotropy for the MMCs, the plastic zones are elongated in the direction of the fibers. Thus the fibers in front of a

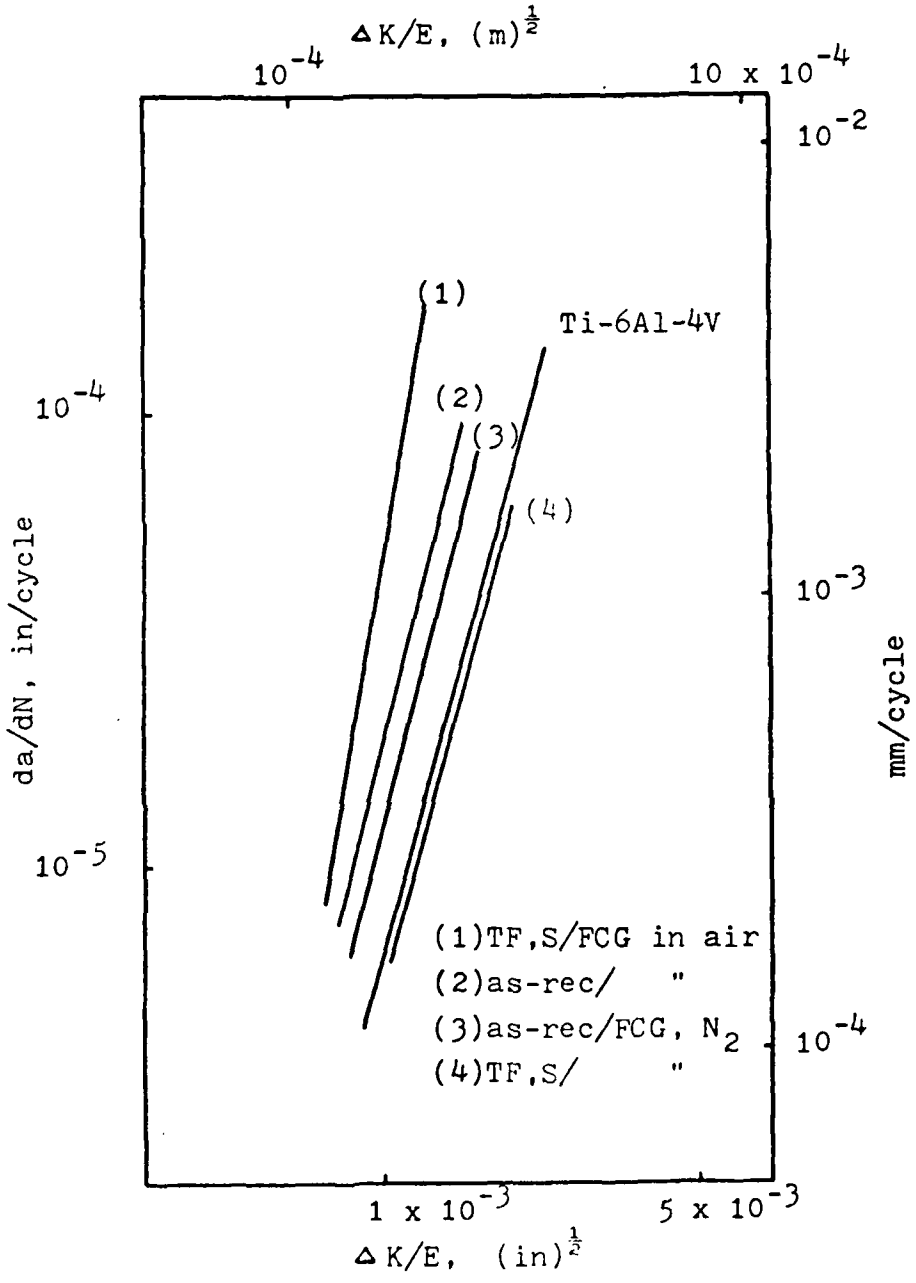

Figure 14. FCG rates after the translation by a factor of 1/0.6, for B_4C/B/Ti-6Al-4V.

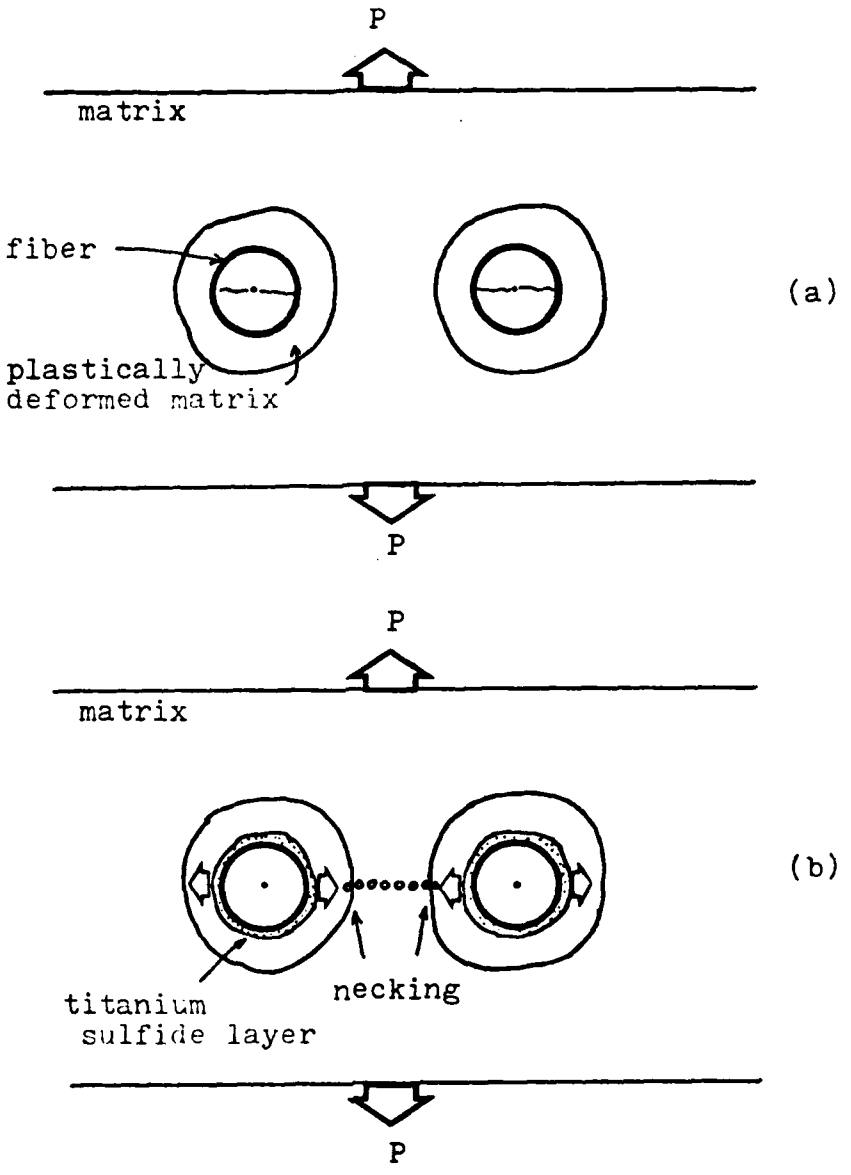

Figure 15. A model for FCG fracture modes in lab air; (a) in as-received; (b) thermal cycled conditions.

sharp crack can be assumed to be surrounded by a plastic sheath of the matrix. During thermal cycling of as-received materials in humid air, the plastically deformed matrix closes over the fibers which do not deform plastically ($\varepsilon_{fiber}=0$). Therefore the fibers suffer pressure and split as discussed earlier (Fig. 15).

In the case of the sulfur enriched specimen, fatigue cycling in humid air reduced the cohesion of the interface. The load is totally carried by the matrix and the necking forms near the matrix side of the interface between the two adjacent fibers since it initiates from the rough crack surface due to the interaction of the titanium sulfide and the humidity in air. Such rough surfaces come from the radial and branch cracks, as shown in Fig. 4 in Appendix A. Figure 15 is a schematic representation of this proposed crack propagation model. The fracture mode is totally interface debonding and the fibers are undamaged as shown in Fig. 11. The high surface mobility of sulfur into the interface is one mechanism that can account for an increased crack growth rate. It is also possible that the necking left behind the more rapidly advancing interface fracture and that the more severe mechanical loading conditions on the matrix cause the increase in FCG.

References

1. D. Mahulikar, "Effect of Environments on the Fatigue Crack Propagation Behavior of Titanium Metal Matrix Composites," PhD Dissertation, The University of Texas, Austin, December 1981.

2. R.J. Bucci, et al., ASTM-STP 513, 1972, p. 125.

3. R.W. Hertzberg, in Deformation and Fracture Mechanics of Engineering Materials, John Wiley, 1976, p. 514.

Appendix D

The Influence of Interfacial Segregation on Cohesion of Interface in Composite Material

Recently, Stark and Marcus[1] have developed a thermodynamic model which describes the change in the grain boundary cohesive energy resulting from solute grain boundary segregation based upon a detailed nonequilibrium thermodynamic analysis of the grain boundary segregation process. In this appendix, the Stark and Marcus model will be modified to apply to composite materials. In the following analysis, most of the basic assumptions used for the Stark and Marcus model will be adopted with some other assumptions which are suitable for the nature of composite materials.

The total Gibb's free energy of the multicomponent system which consists of matrix (M), interface (I) and fiber (F) as shown in Figure 1 is given by[2]:

$$G^T = \sum_j^n \sum_\alpha \mu_j^\alpha N_j^\alpha + \sigma^I A^I \qquad (1)$$

where μ_j^α is the chemical potential of component j in α (=M, I or F), N_j^α is the number of moles of component j in α, σ^I is the surface tension of I and A^I is the surface area of I. If one assumes that F is made of pure element and defines that the component 1 is the solvent in M, the components 2 ~ n-1 are the solutes in M and the component n is the element of pure solid F, one may rewrite eq. 1 as:

$$G^T = \sum_j^{n-1} \sum_\tau \mu_j^\tau N_j^\tau + \mu_{no}^F N_n^F + \sigma^I A^I \qquad (2)$$

where τ is M or I and μ_{no}^F is the standard chemical potential of the component n in F.

Assuming that interfacial segregation takes place at constant interface area, temperature and pressure, and that entropy production due to flow processes is negligible, and that no flux occurs between F and M and between F and I, one may describe the change in the total Gibb's free energy associated with the interfacial segregation process as:

$$\partial G^T = G^{fT} - G^{iT}$$

$$= \sum_{j}^{n-1} \sum_{\tau} (\mu_j^{f\tau} N_j^{f\tau} - \mu_j^{i\tau} N_j^{i\tau}) + (\mu_{no}^{fF} N_n^{fF} - \mu_{no}^{iF} N_n^{iF})$$

$$+ (\sigma^{fI} - \sigma^{iI}) A^I \qquad (3)$$

where superscripts i and f indicate the initial state and the final state of the interfacial segregation process, respectively. Since $\mu_{no}^{iF} = \mu_{no}^{fF}$ and $N_n^{iF} = N_n^{fF}$, eq. 3 can be rewritten as:

$$\partial G^T = \sum_{j}^{n-1} \sum_{\tau} (\mu_j^{f\tau} N_j^{f\tau} - \mu_j^{i\tau} N_j^{i\tau}) + (\sigma^{fI} - \sigma^{iI}) A^I \qquad (4)$$

If one defines that $\partial N_j^{\tau} = N_j^{f\tau} - N_j^{i\tau}$ and $\partial \sigma^I = \sigma^{fI} - \sigma^{iI}$, one may rewrite eq. 4 as:

$$\partial G^T = \sum_{j}^{n-1} \sum_{\tau} [\mu_j^{f\tau} \partial N_j^{\tau} + (\mu_j^{f\tau} - \mu_j^{i\tau}) N_j^{i\tau}] + A^I \partial \sigma^I \qquad (5)$$

Assuming that interfacial segregation is the process from an equal composition state of M and I to an equal chemical potential state of M and I (i.e., the initial state is not an equilibrium state but the composition of I is the same as that of M; whereas the final state is an equilibrium state so that the chemical

potential of I is equal to that of M), one may find:

$$X_j^{iI} = X_j^{iM} \tag{6}$$

$$\mu_j^{fI} = \mu_j^{fM} \tag{7}$$

where X_j^{τ} is the mole fraction of component j in τ. Substituting eq. 7 into eq. 5 one obtains:

$$\partial G^T = \sum_j^{n-1} \sum_{\tau} [\mu_j^{fM} \partial N_j^{\tau} + (\mu_j^{fM} - \mu_j^{i\tau}) N_j^{i\tau}] + A^I \partial \sigma^I \tag{8}$$

Since mass is conserved during the process (i.e., $\sum_{\tau} \partial N_j^{\tau} = 0$), the first term in eq. 8, $\sum_j^{n-1} \sum \mu_j^{fM} \partial N_j^{\tau}$, can be canceled:

$$\partial G^T = \sum_j^{n-1} \sum_{\tau} (\mu_j^{fM} - \mu_j^{i\tau}) N_j^{i\tau} + A^I \partial \sigma^I \tag{9}$$

Now, if one considers the chemical potential in M and I, one finds that due to the presence of surface tension in I the expression of the chemical potential in I will be different from that in M:

$$\mu_j^M = \mu_{jo}^M + RT \ln \gamma_j^M X_j^M \tag{10}$$

$$\mu_j^I = \mu_{jo}^I + RT \ln \gamma_j^I X_j^I - \sigma^I W_j^I \tag{11}$$

where γ_j is the activity coefficient of j and W_j is the partial molar area of j. Assuming that solutes segregating from M to I are sufficiently dilute in M to obey Henry's law in M, one may find that

the activity coefficients in M, γ_j^M, are no longer a function of concentrations, X_j^M. Hence, the final chemical potentials in M can be expressed as:

$$\mu_j^{fM} = \mu_j^{iM} + RT \ln \frac{X_j^{fM}}{X_j^{iM}} \tag{12}$$

Substituting eq. 12 into eq. 9, one obtains:

$$\partial G^T = \sum_j^{n-1} \sum_\tau (RT \ln \frac{X_j^{fM}}{X_j^{iM}} + \mu_j^{iM} - \mu_j^{i\tau}) N_j^{i\tau} + A^I \partial\sigma^I$$

$$= \sum_j^{n-1} N_j RT \ln \frac{X_j^{fM}}{X_j^{iM}} + \sum_j^{n-1} (\mu_j^{iM} - \mu_j^{iI}) N_j^{iI}$$

$$+ A^I \partial\sigma^I \tag{13}$$

From equations 10 and 11 the difference between μ_j^{iM} and μ_j^{iI} can be easily found as:

$$\mu_j^{iM} - \mu_j^{iI} = \mu_{jo}^{iM} - \mu_{jo}^{iI} + RT \ln \frac{\gamma_j^{iM} X_j^{iM}}{\gamma_j^{iI} X_j^{iI}} + \sigma^{iI} W_j^{iI} \tag{14}$$

By substituting eq. 6 into eq. 14 and by defining $\mu_{j*} = \mu_{jo} + RT \ln \gamma_j$ and $\partial\mu_{j*}^{iI} = \mu_{j*}^{iM} - \mu_{j*}^{iI}$, one obtains:

$$\mu_j^{iM} - \mu_j^{iI} = \partial\mu_{j*}^{iI} + \sigma^{iI} W_j^{iI} \tag{15}$$

Hence, eq. 13 can be rewritten as:

$$\partial G^T = \sum_j^{n-1} N_j RT\ell n \frac{X_j^{fM}}{X_j^{iM}} + \sum_j^{n-1} N_j^{iI} \partial \mu_{j*}^{iI}$$

$$+ \sum_j^{n-1} \sigma^{iI} W_j^{iI} N_j^{iI} + A^I \partial \sigma^I \qquad (16)$$

Since $\sum_j^{n-1} W_j^{iI} N_j^{iI} = A^{iI} = A^I$ and $\sigma^{iI} A^I + A^I \partial\sigma^I = (\sigma^{iI} + \partial\sigma^I) A^I = \sigma^{fI} A^I$, one finally obtains:

$$\partial G^T = \sum_j^{n-1} N_j RT\ell n \frac{X_j^{fM}}{X_j^{iM}} + \sum_j^{n-1} N_j^{iI} \partial \mu_{j*}^{iI} + \sigma^{fI} A^I \qquad (17)$$

However, from the definition of the Gibb's free energy (i.e., G=H-TS), the total Gibb's free energy change of the above process can also be expressed as:

$$\partial G^T = \partial H^T - T\partial S^T \qquad (18)$$

where H^T and S^T are total enthalpy and entropy of the system, respectively. By comparing eqs. 17 and 18, one can find that the first term in eq. 17, $\sum_j^{n-1} N_j RT\ell n \frac{X_j^{fM}}{X_j^{iM}}$, is associated with the configurational entropy change of the process, while the last two terms in eq. 17, $\sum_j^{n-1} N_j^{iI} \partial \mu_{j*}^{iI} + \sigma^{fI} A^I$ account for the enthalpy and vibrational entropy changes of the process. Hence, if for simplicity, one removes the vibrational entropy change from the last two terms in eq. 17, one can rewrite eq. 17 as:

$$\partial G^T = \partial H_o^I + \sigma^{fI} A^I - T\partial S^T \qquad (19)$$

It can be seen from eqs. 15, 17 and 19 that ∂H_o^I is the enthalpy change associated with the transformation of I at its initial concentration into M without a concentration change. By defining that $\partial H_\star^I = \partial H_o^I + \sigma^{fI} A^I$, one obtains:

$$\partial G^T = \partial H_\star^I - T\partial S^T \tag{20}$$

From eqs. 18 and 20, the total enthalpy change of the process can be found as:

$$\partial H^T = \partial H_\star^I \tag{21}$$

Now, ∂H^T compares to a transformation of material from an initial state of high measured surface tension to a hypothetical final state of reduced surface tension without concentration change.

Since enthalpy is an extensive variable, the total enthalpy change of the system may be given by the sum of the enthalpy change in each region:

$$\partial H^T = \partial H^M + \partial H^I + \partial H^F \tag{22}$$

Here, the main consideration is determining the enthalpy change in I during interfacial segregation. Hence, rearranging eq. 22, one obtains:

$$\partial H^I = \partial H^T - \partial H^M - \partial H^F \tag{23}$$

Since ∂H^T was already evaluated as eq. 21, what must be considered here is ∂H^M and ∂H^F.

As an extensive variable, enthalpy in M obeys Euler's theorem:

$$H^M = \sum_j^{n-1} \bar{H}_j^M N_j \tag{24}$$

where $\bar{H}_j^M$ is the partial molar enthalpy of component j in M. Hence, the enthalpy change in M can be written as:

$$\partial H^M = H^{fM} - H^{iM}$$

$$= \sum_j^{n-1} (\bar{H}_j^{fM} N_j^{fM} - \bar{H}_j^{iM} N_j^{iM}) \tag{25}$$

However, solutes in M are sufficiently dilute to follow Henry's law which implies that:

$$\bar{H}_1^{fM} = \bar{H}_1^{iM} = \bar{H}_1^M = \underline{H}_1^M \tag{26}$$

$$\bar{H}_j^{fM} = \bar{H}_j^{iM} = \bar{H}_j^M \quad \text{for } j=2 \text{ to } n-1 \tag{27}$$

where $\underline{H}_1^M$ is the specific enthalpy of pure solvent 1 in M. Combining eqs. 25, 26 and 27, one obtains:

$$\partial H^M = \underline{H}_1^M \partial N_1^M + \sum_{j=2}^{n-1} \bar{H}_j^M \partial N_j^M \tag{28}$$

Since fiber is made of pure element n, the enthalpy of F can be expressed as:

$$H^F = \underline{H}_n^F N_n^F \tag{29}$$

Hence, the enthalpy change in F is:

$$\partial H^F = \underline{H}_n^{fF} N_n^{fF} - \underline{H}_n^{iF} N_n^{iF} \tag{30}$$

However, $\underline{H}_n^{fF} = \underline{H}_n^{iF}$ and $N_n^{fF} = N_n^{iF}$ since no flux occurs between F and M and between F and I. Therefore, the enthalpy change in F is zero:

$$\partial H^F = 0 \tag{31}$$

Finally, combining eqs. 21, 23, 28 and 31, one may find the equation which describes the enthalpy change in I associated with interfacial segregation:

$$\partial H^I = \partial H_\star^I - \underline{H}_1^M \partial N_1^M - \sum_{j=2}^{n-1} \overline{H}_j^M \partial N_j^M \tag{32}$$

Therefore, the effect of interfacial segregation on the cohesion of interface in composite materials can be numerically evaluated by using eq. 32 with the proper assumption on the term $\partial H_\star^I$ and the published data on $\underline{H}_1^M$ and $\overline{H}_j^M$.

Following Stark and Marcus[1] the term $\partial H_\star^I$ can be assumed to be -22 kJ/mole, the specific enthalpy $\underline{H}_1^M$ may be substituted with the negative values of the published thermodynamic data on the sublimation enthalpy of pure solvent 1, and the partial molar enthalpy $\overline{H}_j^M$ can be calculated by using the phase diagram and the solubility data of the solute j in the solvent 1. The analysis on the interface embrittlement problems associated with impurity interface segregation in the Ti matrix composite material is being conducted now.

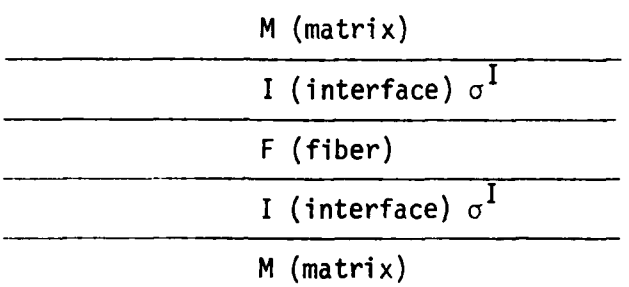

Figure 1. The model of interface region in composite material

References

1. J.P. Stark and H.L. Marcus, Met. Trans. 8A (1977), pp. 1423-1429.

2. M. Guttmann, Surf. Sci. 53 (1975), pp. 213-227.

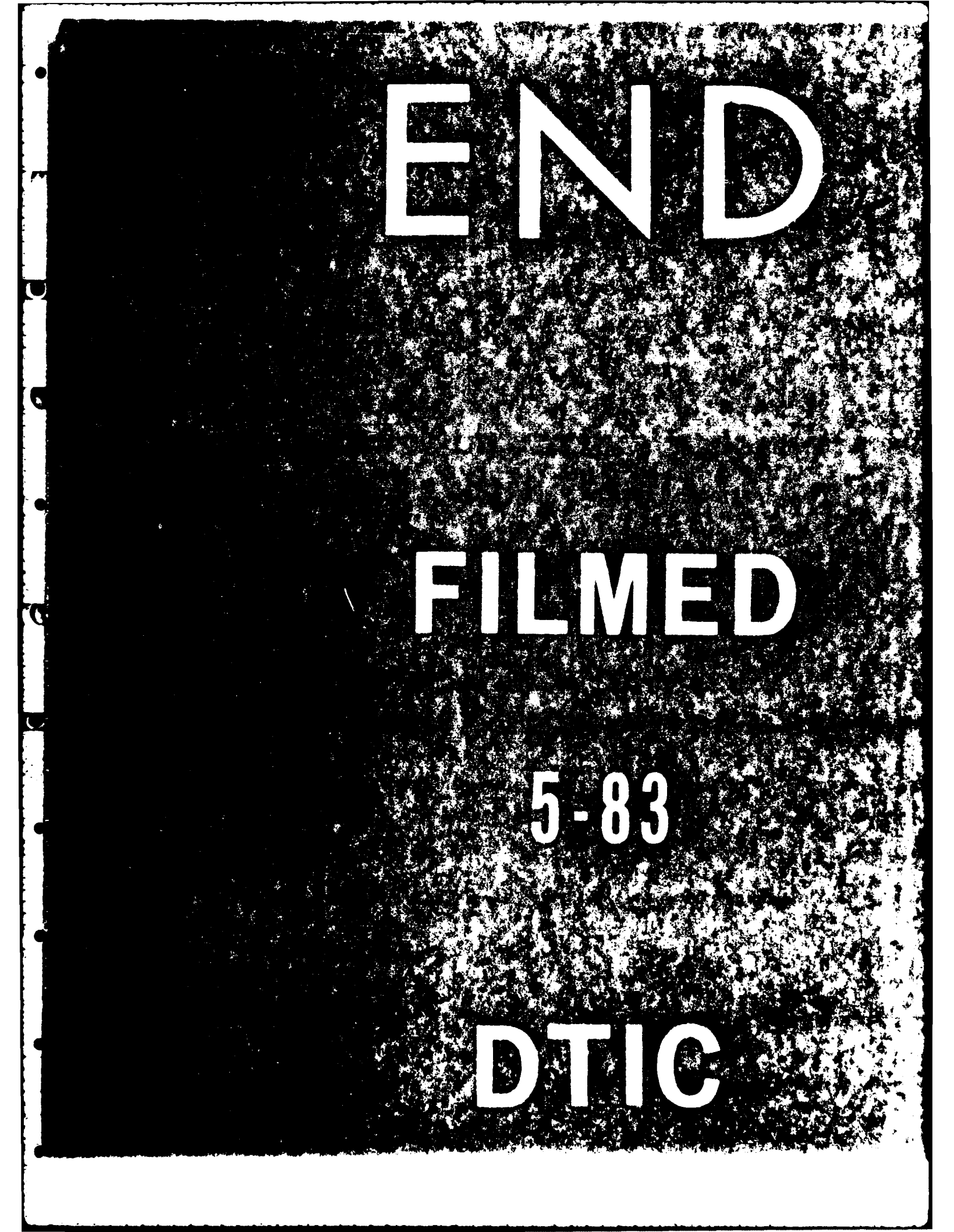
END
FILMED
5-83
DTIC